American Mineralogist, Volume 72, pages 879–901, 1987

Mineralogy of the Wooley Creek batholith, Slinkard pluton, and related dikes, Klamath Mountains, northern California

Calvin G. Barnes
Department of Geosciences, Texas Tech University, Lubbock, Texas 79409, U.S.A.

Abstract

The Wooley Creek batholith and Slinkard pluton are part of a vertically extensive plutonic system exposed by tilting and erosion. In general, the system is upwardly zoned from pyroxene gabbro to biotite + hornblende granite. Structurally highest levels of the system consist of numerous roof-zone dikes that range from basaltic to dacitic compositions and represent fractions of magma tapped from the underlying magma. Comparison of mineral compositional and zoning patterns suggests that andesitic dikes have cognate plutonic rocks in the deep levels of the system (lower Wooley Creek batholith and Slinkard pluton) whereas dacitic dikes have cognate plutonic rocks in the upper Wooley Creek batholith. Basaltic roof-zone dikes have few coarse-grained equivalents in the system except for mafic selvages, cumulate gabbroic blocks, mafic enclaves, and synplutonic mafic dikes. Various mineral equilibria provide estimates of intensive variables during cooling of the system. Pyroxene and oxide compositions in andesitic rocks indicate temperatures in the range 912°C to 1120°C with f_{O_2} slightly higher than NNO. Hornblende and biotite compositional trends also suggest that differentiation was accompanied by oxidation. The presence of primary titanite and relatively Mg-rich mafic phases in a late-stage granite stock indicates intrinsic oxidation of the youngest magmas in the system. Mineral parageneses among the entire suite suggest H_2O-rich but undersaturated conditions. The effect of pressure on pyroxene and hornblende compositions is primarily seen as a minor increase in Al content. Plagioclase zoning patterns suggest that magma mixing primarily resulted in chemical buffering of the system until the magma volume was small enough to be strongly affected by influx of basalt.

Introduction

Numerous studies of ash-flow deposits have shown that the upper parts of many magma bodies are compositionally and mineralogically zoned (e.g., Williams, 1942; Smith, 1979; Christiansen et al., 1977; Hildreth, 1981). Eruption of voluminous, phenocryst-poor rhyolitic ash flows suggests the presence of a vertically extensive mafic root beneath the system that supplies heat, volatiles, and fractionated liquid to the upper, high-silica magma (e.g., Smith, 1979; Hildreth, 1981). Petrologic and geophysical studies of granitoid batholiths have led to the conclusion that many batholiths are underlain by dense mafic rock that represents the crystallized root zone of the magma system (e.g., Bateman and Chappell, 1979; Bateman and Eaton, 1967). However, few granitoid plutons are dissected deeply enough to expose appreciable mineralogical or compositional variation. In some cases, geologic, petrologic, and geophysical evidence can be used to demonstrate that a plutonic body has been tilted (Flood and Shaw, 1979; Cater, 1982; Barnes, 1983; Barnes et al., 1986b; Dellinger and Hopson, 1986) such that subsequent erosion has exposed a significant "vertical" structural section of the pluton.

The Wooley Creek batholith and Slinkard pluton (WCB-SP) are the upper and lower parts, respectively, of a vertically extensive plutonic system in the Klamath Mountains of northern California (Barnes et al., 1986a, 1986b). The system is gradationally zoned from structurally lowest two-pyroxene gabbro to structurally highest biotite + hornblende granodiorite and granite (Barnes, 1983; Barnes et al., 1986a). In addition, the wall rocks adjacent to the highest structural levels (the "roof zone") were cut by numerous dikes derived from the underlying magma chamber. These dikes provide samples of the evolving magma that did not undergo the prolonged cooling history experienced by the plutons. This paper reports an investigation into the compositional variations among the mineral phases in the WCB-SP system, the effects of slow cooling on mineral compositions, an attempt to relate the roof-zone dike rocks to their depth of origin in the system, and an attempt to use mineral equilibria to estimate the intensive variables of crystallization.

Geologic setting

The Klamath Mountain province can be broadly divided into four lithotectonic belts or composite terranes (Irwin, 1960, 1966, 1981). The composite terranes were juxtaposed by east-dipping thrust faults so that, in gen-

0003–004X/87/0910–0879$02.00

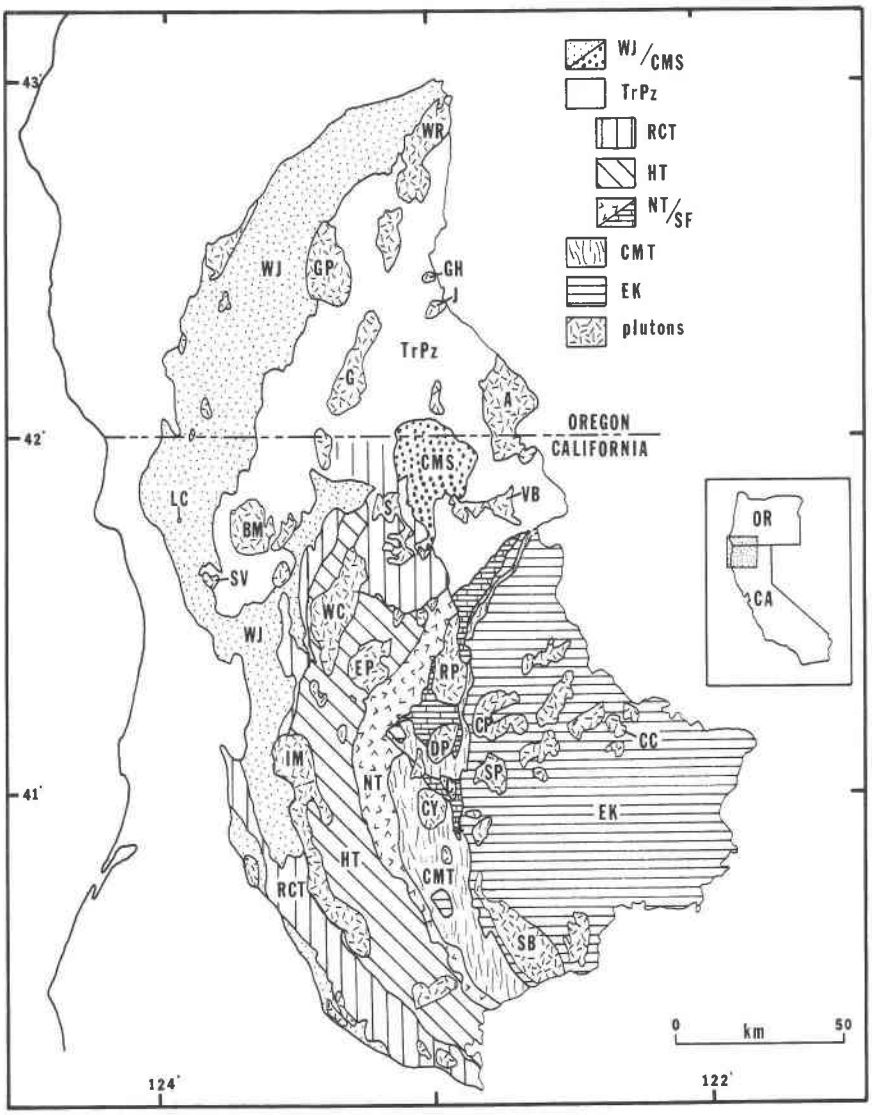

Fig. 1. Simplified geologic map of Klamath Mountain province. WJ, western Jurassic terrane; CMS, Condrey Mountain Schist; TrPz, undivided western Paleozoic and Triassic terrane; RCT, Rattlesnake Creek terrane; HT, Hayfork terranes; NT, North Fork terrane, SF, Stuart Fork Formation; CMT, Central Metamorphic terrane; EK, Eastern Klamath terrane. WC, Wooley Creek batholith; S, Slinkard pluton; see Irwin (1985) for identification of other plutons. After Irwin (1981).

eral, terranes to the west are younger than those to the east (Irwin, 1981). From east to west, the composite terranes are the Eastern Klamath, the Central Metamorphic, the western Paleozoic and Triassic, and the western Jurassic (Fig. 1). The western Paleozoic and Triassic composite terrane is host to the WCB-SP and consists of at least five terranes (Irwin, 1972) that are also separated by east-dipping thrust faults. These terranes are, from east to west, the Stuart Fork Formation (Fort Jones terrane of Blake et al., 1982), the North Fork terrane, the eastern Hayfork terrane, the western Hayfork terrane, and the Rattlesnake Creek terrane (Irwin, 1972; Wright, 1982; Fig. 1). The high-grade equivalent of the Rattlesnake Creek terrane was named the Marble Mountain terrane by Blake et al. (1982); however, the name Rattlesnake Creek terrane was retained by Coleman et al. (1987) in a recent synthesis of the metamorphic history of the area. The WCB-SP intruded the high-grade Rattlesnake Creek terrane, western Hayfork terrane, and eastern Hayfork terrane at approximately 162 Ma (Barnes et al., 1986a). The Slinkard pluton is intrusive only into the structurally lowest high-grade Rattlesnake Creek terrane, whereas the Wooley Creek batholith crosscuts all three units (Fig. 1).

During the Nevadan orogeny (approximately 150 Ma, Harper and Wright, 1984), rocks of the western Jurassic belt were thrust beneath the western Paleozoic and Triassic belt and its associated plutons. Gravity studies (Jachens et al., 1986; Mortimer, 1985) show that rocks of the

western Paleozoic and Triassic belt and WCB-SP are underlain by low-density rocks of the western Jurassic belt and Condrey Mountain Schist (Fig. 1) as much as 70 km east of the study area. Post-Nevadan doming of the Condrey Mountain Schist (Mortimer and Coleman, 1985) tilted the overlying western Paleozoic and Triassic belt so that erosion has exposed the structurally deepest levels of the western Paleozoic and Triassic belt adjacent to the dome.

The effects of tilting of the WCB-SP are seen as a decrease in the estimated pressure of contact metamorphism from northeast to southwest (Barnes, 1983; Barnes et al., 1986b). Barnes et al. (1986b) estimated a contact metamorphic pressure of ~6.5 kbar at the northern contact of the Wooley Creek batholith, ~3.5 kbar near the western contact, and 3 kbar at the southern contact. These estimates result in an estimated structural relief of ~9 km in the Wooley Creek batholith and as much as 12 km in the entire system.

Summary of compositional zoning of the WCB-SP

The Slinkard pluton is a sill-like body that lies on the southwestern flank of the Condrey Mountain dome and dips southwest away from the dome (Barnes et al., 1986a). The base of the Slinkard pluton is locally marked by a ductilely deformed quartz diorite and elsewhere by a narrow zone of two-pyroxene gabbro and hornblende gabbro (Fig. 2). The pluton grades upward to weakly foliated biotite + hornblende quartz diorite. The southwestern part of the Slinkard pluton grades upward to a southwest-dipping protoclastic biotite + hornblende tonalite, whereas the northern part is underlain by an unfoliated muscovite + biotite granodiorite and granite. Xenoliths are rare in the Slinkard pluton except near contacts. Mafic microgranitoid enclaves are sparse or absent. Rare porphyritic two-pyroxene gabbro dikes occur within the Slinkard pluton.

The structurally deepest (northeastern) part of the Wooley Creek batholith consists of protoclastic biotite + hornblende quartz diorite and tonalite that dip northeast toward the protoclastic tonalite of the Slinkard pluton (Fig. 2). The Wooley Creek batholith grades upward (southwestward) to two-pyroxene gabbro, biotite + hornblende + pyroxene gabbro and quartz diorite, and biotite hornblende granodiorite, tonalite, granodiorite, and granite (Barnes, 1983). The upper granodiorite and granite are intruded by a stock composed of medium- to fine-grained, locally aplitic hornblende + biotite granodiorite and granite (Fig. 2). The central structural level of the Wooley Creek batholith is a zone in which coarse- to fine-grained mafic dikes and mafic microgranitoid enclaves are locally abundant (Fig. 2). This zone markes a gradual transition from structurally lower pyroxene-bearing rocks to structurally higher pyroxene-free rocks and a relatively sharp transition in whole-rock compositional trends (Barnes, 1983). Barnes (1983) and Barnes et al. (1986a) suggested that this zone represents a compositional interface in the WCB-SP magma that acted as a density trap for high-temperature basaltic magma injected from below. They suggested that at least some of the mafic microgranitoid enclaves are disrupted hybrids of injected mafic magmas.

Xenoliths are conspicuous in a zone 1 to 2 km wide adjacent to the northeastern and eastern contacts. Xenolith lithologies reflect those of the host rocks and range from rare quartzite and pelitic rocks to common mafic hornfels. Near the northeastern contact, xenoliths of peridotite, amphibolite, and rare garnet + hornblende gabbro crop out. The largest xenoliths have maximum dimensions of several tens of meters, but maximum dimensions of 3 to 5 m are typical. A few centimeter-scale xenoliths were recognized in the field; most are siliceous or calcareous.

Wooley Creek batholith roof zone

The wall rocks of the Wooley Creek batholith along the southern and southwestern contact were invaded by numerous porphyritic dikes during intrusion of the batholith (roof-zone dikes). Barnes et al. (1986a) presented petrographic, compositional, and geochronologic evidence that demonstrated the cogenetic relationship between the roof-zone dikes and the Wooley Creek batholith. They showed that the general sequence of dike intrusion was aphyric and clinopyroxene-phyric basalt, two-pyroxene andesite, biotite + hornblende dacite, pegmatite and aplite, two-pyroxene and clinopyroxene + hornblende andesite, biotite + hornblende dacite, and pegmatite. Final emplacement and crystallization of the roof-zone granodiorite of the Wooley Creek batholith followed intrusion of the first biotite + hornblende dacitic dikes. Barnes et al. (1986a) interpreted the sequence of intrusion to indicate that magma of intermediate composition remained in deep levels of the system after granodiorite of the roof-zone had crystallized.

Barnes et al. (1986a) recognized that the roof-zone dikes represent samples of the magma of the underlying WCB-SP. As such the dikes are less likely to show the effects of crystal accumulation that are typical of intermediate and felsic plutons (e.g., McCarthy and Hasty, 1976). In addition, the roof-zone dikes were rapidly cooled relative to the plutonic rocks. Therefore, the phenocryst assemblages in the dikes are more likely to represent magmatic conditions, whereas the mineral phases of the plutonic rocks are likely to have equilibrated at lower temperatures during slow cooling. As such, the roof-zone dikes should provide the most useful estimates of temperature, f_{O_2}, and f_{H_2O} during the magmatic history of the system.

Sampling and analytical techniques

Whole-rock analytical techniques were reported by Barnes (1983) for samples (Table 1) from the Wooley Creek batholith, Slinkard pluton, and roof-zone dikes. Additional mafic dike, enclave, and xenolith analyses were done by atomic absorption spectrometry at Texas Tech University (Table 2). Fe^{2+} was determined by titration with ammonium metavanadate.

Mineral compositions were determined by electron microprobe using natural and synthetic mineral standards and a mod-

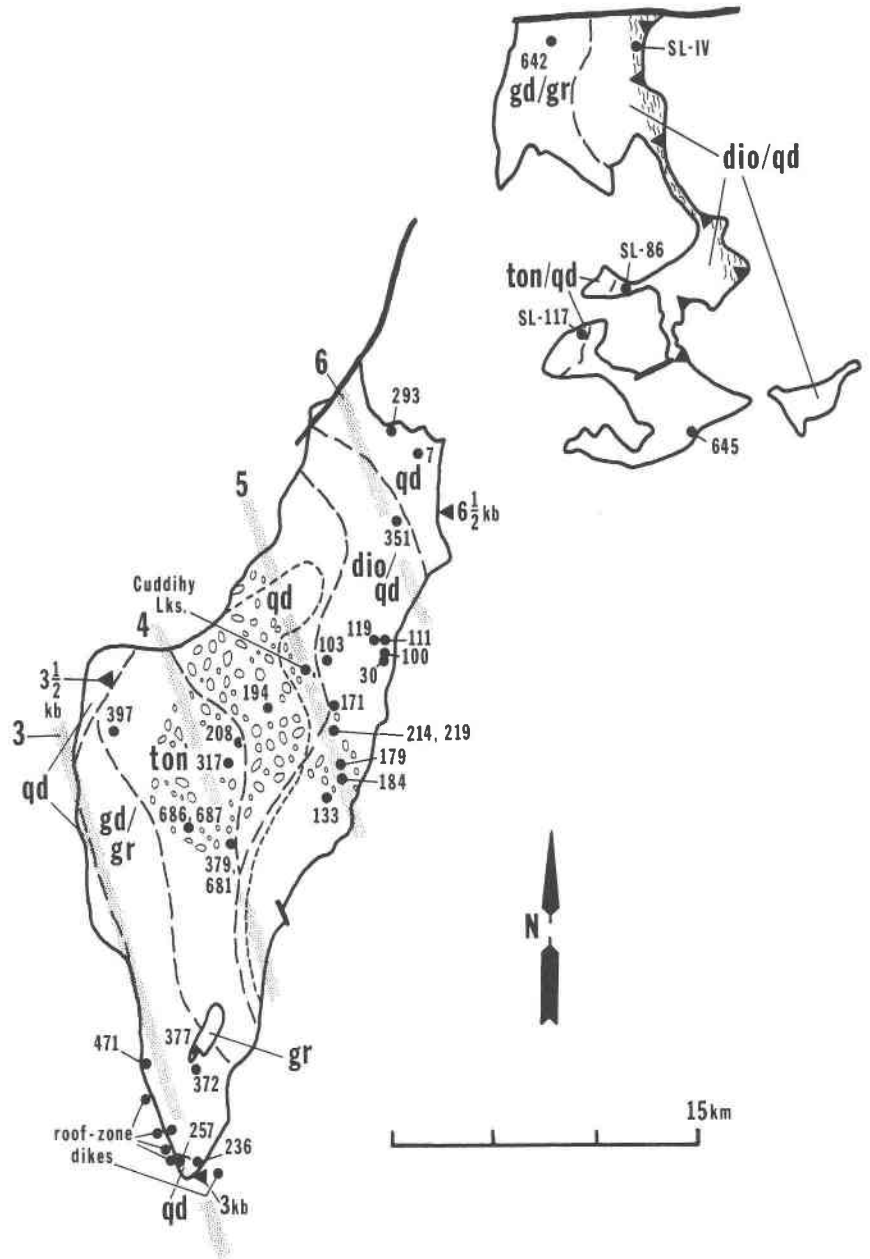

Fig. 2. Map showing compositional zoning and sample locations in the WCB-SP. Long-dashed lines, gradational boundaries between rock types; short-dashed line, gradational contact between lower pyroxene-bearing and upper pyroxene-free parts of the system. Location of samples for which pressure has been estimated (Barnes et al., 1986b) shown by triangles; stippled bands show estimated isobars assuming the WCB was tilted as a single unit (see text). Patterned area in central WCB is enclave-rich zone. Cuddihy Lakes locality includes WCB sample 777B and synplutonic mafic dikes 638, 639, 771, 775, and 776. Note mylonitic zone along eastern contact of SP. After Barnes et al. (1986a).

ified Bence-Albee reduction scheme. Most analyses were carried out at Southern Methodist University on a JEOL JXA-733. Some amphibole data were gathered at the U.S. Geological Survey by J. Hammarstrom. In addition, microprobe data reported by Barnes (1982, 1983) were incorporated into the data set. Replicate analyses indicate that data from all three sources are comparable. Analytical conditions were typically 15-kV accelerating voltage and 20-nA beam current on a 10-μm spot, defocused to 20–40 μm for feldspars. Analytical uncertainties shown in Figures 6 to 7 are based on one standard deviation for multiple analyses of a homogeneous standard mineral.

Petrography

The geologic setting and rock type for the analyzed samples are presented in Table 1. Petrographic descrip-

tions of the WCB-SP rocks were presented by Barnes et al. (1986a), Allen (1981), and Barnes (1982, 1983) and are contained in Appendix 1 of this report.[1] In the remainder of the paper, coarse-grained, slowly-cooled parts of the system will be referred to as "plutonic," whereas "roof-zone dike" will be used to refer to porphyritic to equigranular intrusions in the roof and uppermost part of the Wooley Creek batholith.

Mafic dikes are common in the middle structural level of the Wooley Creek batholith and sparse in the upper and lower structural levels of the system (Barnes, 1983; Barnes et al., 1986a). The dikes range from fine grained to very coarse grained and typically carry sparse phenocrysts of hornblende and plagioclase. Groundmass textures range from idiomorphic granular to hypidiomorphic granular, to (rarely) trachytoid. Groundmass minerals are hornblende + plagioclase ± clinopyroxene ± quartz ± biotite. Magnetite and acicular apatite are common accessory minerals. Coarse-grained mafic dikes are sparse and almost invariably consist of centimeter-scale equant hornblende ± clinopyroxene with interstitital to poikilitic plagioclase ± quartz (e.g., sample 638, App. 1).

Mafic microgranitoid enclaves (Vernon, 1983; Didier, 1973) are commonly associated with the mafic dikes described above and can locally be shown to be the products of disruption of such dikes (Barnes et al., 1986a). The enclaves are similar to the dikes in grain size and texture, but medium-grained porphyritic hypidiomorphic granular texture is most common. Typical phenocryst phases are hornblende and oscillatory-zoned plagioclase. The color index of the mafic microgranitoid enclaves is highly variable, even in a single outcrop. However, mineral assemblages in the enclaves are typically identical to those in the host granitoid (Barnes, 1983; Pabst, 1928). In rare cases, enclaves lacking groundmass quartz are enclosed by a quartz-bearing host. In these cases, the enclaves commonly contain quartz xenocrysts with coronas of fine-grained amphibole (Barnes et al., 1986a). Acicular apatite is a ubiquitous accessory phase in the enclaves, whereas prismatic apatite is typical of the host granitoid. Vernon (1983) interpreted the presence of acicular apatite and of oscillatory-zoned plagioclase in mafic microgranular enclaves to be the result of disruption of undercooled mafic liquids by the host magma. Such an interpretation for the Wooley Creek batholith is also in accord with the field relations cited above (see Barnes, 1983; Barnes et al., 1986a).

Mafic metavolcanic xenoliths range in grain size from fine to medium grained and display hornfelsic, nematoblastic, and idiomorphic granular textures. Pelitic xenoliths have lepidoblastic to granoblastic textures. Typical mineral assemblages are given in Table 1. Rare garnet metagabbro xenoliths (location 7, Fig. 2) are coarse-grained hypidiomorphic granular to granoblastic with poikiloblasts of garnet and ferro-tschermakitic hornblende (App. 1; Bickner, 1977).

TABLE 1. Summary of sample descriptions

Sample no.	Geologic setting*	Rock type**
IV (SLIV)	XP, mylonitic	bio hnbl qd
7B	xenolith, WCB	gt cumm hnbl metagb
30	WCB	bio px qd
86 (SL86)	SP	bio hnbl qtz gb
103	WCB	px bio hnbl qtz gb
111	WCB	bio px qtz gb
117 (SL117)	SP	bio hnbl ton
119B	xenolith, WCB	cpx bio hnbl hnfls
133	xenolith, WCB	hnbl px hnfls
134 (SL134)	SP dike	hnbl px microgb
164	r-z dike	px andesite
171	block in WCB	hnbl pyroxenite
179	xenolith, WCB	px hnfls
184	block in WCB	px gb
194	WCB	bio hnbl qd
208	WCB	bio hnbl qtz md
214	xenolith, WCB	hnbl cpx hnfls
219A	xenolith, WCB	bio cumm hnbl hnfls
219B	xenolith, WCB	bio hnbl px hnfls (+cumm)
219D	xenolith, WCB	crd bio schist
236A	WCB selvage	ol px microgb
257	WCB selvage	px gb
264	SP	hnbl px gb
293	WCB	bio hnbl qd
317	WCB	bio hnbl qtz md
351	WCB	hnbl px dio
372	WCB	bio hnbl gr
377	WCB, late stock	hnbl bio gr
379	WCB	bio hnbl qd
397	WCB	bio hnbl qd
471	WCB	bio hnbl gd
548	r-z dike	(opx) bio hnbl microgd (dacite)
551	r-z dike	bio hnbl microgd (dacite)
553	r-z dike	px andesite
555	r-z dike	ol px basalt (microgb)
557	r-z dike	px andesite
579	r-z dike	bio hnbl gd (dacite)
584	r-z dike	px andesite
590	r-z dike	hnbl basalt (microgb)
638	synplutonic dike	cpx hnbl dio
639	synplutonic dike	cpx bio hnbl gb
642	SP	ms bio gr
645A	SP	hnbl px gb
681A, 681aH	WCB	bio hnbl dio
681aE	WCB, enclave	bio hnbl dio
681B	WCB, enclave	bio hnbl dio
686B	WCB, enclave	bio hnbl qtz gb
686E	WCB, enclave	bio hnbl qd
687	WCB	bio hnbl gd
693	r-z dike	cpx hnbl andesite
697	r-z dike	bio hnbl microgd (dacite)
699	r-z dike	px andesite
704	r-z dike	px andesite
766	WCB, enclave	bio hnbl gb
771	synplutonic dike	bio hnbl gb
775A	synplutonic dike	cpx bio hnbl gb
776	synplutonic dike	hnbl gb
777B	WCB	px bio hnbl qd

* SP, Slinkard pluton; WCB, Wooley Creek batholith; r-z, roof zone.
** gt, garnet; cumm, cummingtonite; bio, biotite; px, pyroxene; hnbl, hornblende; qtz, quartz; ol, olivine; ms, muscovite; crd, cordierite; gb, gabbro; dio, diorite; qd, quartz diorite; md, monzodiorite; ton, tonalite; gd, granodiorite; gr, granite; hnfls, hornfels.

MINERAL COMPOSITIONS

Olivine

Olivine is rare in the WCB-SP. It occurs in hornblende olivine (Fo_{71}) pyroxenite blocks that Barnes (1983) inter-

[1] To obtain a copy of Appendix 1, order Document AM-87-354 from the Business Office, Mineralogical Society of America, 1625 I Street, N.W., Suite 414, Washington, D.C. 20006, U.S.A. Please remit $5.00 in advance for the microfiche.

TABLE 2. Representative major-element analyses

Sample	SiO_2	TiO_2	Al_2O_3	Fe_2O_3	FeO	MnO	MgO	CaO	Na_2O	K_2O	P_2O_5	LOI	Total
638	55.43	0.52	7.18	1.51	7.31	0.17	12.06	11.84	1.08	0.59	0.07	1.44	99.20
639	50.18	1.84	17.58	1.26	7.80	0.16	6.83	9.86	2.58	0.88	0.29	0.90	100.16
766	51.39	0.83	14.11	10.31	n.d.	0.20	7.81	10.53	2.51	0.74	0.17	1.03	99.63
681B	48.78	0.90	16.22	12.36	n.d.	0.21	7.11	9.52	2.65	1.04	0.21	1.38	100.38
686B	56.00	1.20	16.97	5.05	2.81	0.16	4.94	7.27	3.16	1.29	0.22	1.22	100.29
686E	55.51	0.74	16.73	0.00	10.06	0.13	4.77	6.97	3.04	1.32	0.22	1.20	100.69
557	59.12	0.61	16.00	1.33	5.56	0.15	4.52	6.79	2.92	1.99	0.20	0.92	100.11
579	71.92	0.24	14.33	0.05	1.66	0.04	0.88	2.05	2.65	4.72	0.04	0.39	98.97
693	60.70	0.81	15.67	0.37	6.37	0.11	4.16	5.17	3.43	2.28	0.16	1.62	100.85
699	62.07	0.96	16.74	1.60	4.64	0.09	1.95	4.87	3.06	3.06	0.27	0.70	100.01
681Ah	60.80	1.07	16.36	1.90	5.04	0.15	3.95	6.42	2.73	1.11	0.20	1.49	101.22
687	59.24	0.76	15.23	2.00	5.60	0.14	4.38	6.24	3.01	2.31	0.19	0.83	99.93
642A	74.88	0.24	14.23	0.23	1.19	0.03	0.20	1.60	3.97	2.74	0.01	0.44	99.76
645A	55.27	0.62	17.38	0.20	8.29	0.16	5.93	9.28	2.29	0.19	0.05	0.13	99.79

preted as disrupted cumulates. In addition, olivine (Fo_{45}) is present in a porphyritic, fine-grained biotite + olivine + clinopyroxene gabbro (sample 236A) at the eastern contact of the roof-zone (Fig. 2). Ca contents in these olivines suggest that they were in equilibrium with a magma and were not xenocrysts from peridotites in the wall rocks (Barnes, 1983; Watson, 1979).

Pyroxene

In the Slinkard pluton, pyroxene occurs in two-pyroxene gabbro (± hornblende) near the eastern contact of the pluton (samples 264 and 645A) and as sparse clinopyroxene cores in hornblende in structurally higher quartz diorite and tonalite (SL86). The Wooley Creek batholith can be divided into pyroxene-bearing and pyroxene-free zones along a gradational boundary shown in Figure 2 (Barnes, 1983). Clino- and orthopyroxenes are also present in mafic selvages adjacent to the roof zone (e.g., samples 236A, 257A; Fig. 2) and as cores in hornblende in shallow parts of the pluton. Typical pyroxene-bearing rock types are listed in Table 1. Most roof-zone dikes are pyroxene-bearing. Compositions range from clinopyroxene-phyric basalt, through two-pyroxene andesite, to clinopyroxene + hornblende andesite. Rare orthopyroxene cores in hornblende are present in some biotite + hornblende dacite dikes (Table 1). Pyroxenes are sparse in synplutonic mafic dikes and mafic microgranitoid enclaves within the Wooley Creek batholith. Where present, they are subhedral and show reaction to hornblende.

Clinopyroxene and orthopyroxene in the coarse-grained plutonic rocks typically show reaction to hornblende; however, some samples from the east-central Wooley

TABLE 3. Representative average pyroxene analyses

	Orthopyroxene						Clinopyroxene			
	704	584	548	111	100	645A	704	584	555	397
	Compositions in wt%									
SiO_2	53.64	53.97	51.36	50.97	54.54	51.49	52.04	52.30	51.78	52.53
TiO_2	0.22	0.23	0.09	0.25	0.17	0.07	0.47	0.48	0.53	0.10
Al_2O_3	0.88	0.94	0.64	1.15	2.12	1.21	1.70	1.95	2.71	0.83
MnO	0.54	0.48	1.32	0.58	0.22	0.58	0.31	0.30	0.30	0.59
FeO	20.12	18.87	29.92	25.01	13.75	26.40	9.97	9.61	9.95	9.90
MgO	23.52	24.94	16.38	20.43	27.29	18.84	14.94	15.08	15.30	12.78
CaO	1.44	1.49	0.81	1.50	1.70	1.44	20.23	18.94	19.37	22.50
Na_2O	0.02	0.04	0.01	0.06	0.09	0.03	0.34	0.31	0.29	0.38
Cr_2O_3	0.04	0.10	0.15	0.05	0.09	0.02	0.08	0.16	0.09	0.06
Total	100.35	101.05	100.64	99.98	99.96	100.11	100.07	99.12	100.33	99.63
	Cations per six oxygens*									
Si	1.974	1.958	1.980	1.931	1.955	1.957	1.935	1.958	1.916	1.978
Ti	0.006	0.006	0.003	0.007	0.005	0.001	0.013	0.014	0.015	0.003
^{IV}Al	0.026	0.038	0.020	0.052	0.046	0.042	0.065	0.042	0.084	0.022
^{VI}Al	0.012	0.002	0.009	0.000	0.045	0.012	0.009	0.044	0.034	0.015
Mn	0.017	0.015	0.043	0.019	0.007	0.018	0.010	0.010	0.009	0.019
Fe^{2+}	0.614	0.550	0.957	0.753	0.412	0.812	0.260	0.301	0.270	0.284
Fe^{3+}	0.003	0.023	0.008	0.040	0.000	0.027	0.050	0.000	0.038	0.028
Mg	1.289	1.348	0.939	1.153	1.457	1.066	0.827	0.841	0.843	0.717
Ca	0.057	0.058	0.033	0.061	0.065	0.058	0.805	0.759	0.769	0.908
Na	0.001	0.003	0.001	0.004	0.006	0.002	0.023	0.023	0.021	0.027
Cr	0.001	0.003	0.004	0.002	0.003	0.000	0.003	0.004	0.003	0.002
Total	4.001	4.004	3.998	4.019	3.998	4.000	4.001	3.995	4.002	4.001

* Calculated according to Lindsley and Andersen (1983).

Creek batholith show reaction to biotite. Most pyroxene crystals from the coarse-grained rocks show fine- to medium-scale exsolution lamellae. In general, only samples with very thin lamellae were analyzed, and the data from several spot analyses were averaged to yield the data given in Table 3. Pyroxenes from the roof-zone dikes contain very thin lamellae or lack visible exsolution lamellae. Pyroxene in roof-zone dikes is euhedral and without reaction rims, or shows reaction to hornblende. Orthopyroxene is commonly rimmed by clinopyroxene in both the biotite + pyroxene gabbro and quartz diorite and in roof-zone dikes (App. 1). However, individual samples contain orthopyroxene crystals with and without clinopyroxene rims. Clinopyroxene (Fe-rich augite to ferrosalite) is the predominant pyroxene in hornfelsic xenoliths. It typically lacks exsolution lamellae or is weakly exsolved and shows reaction to calcic amphibole and/or cummingtonite.

Average pyroxene compositions are listed in Table 3 and plotted in Figure 3. Mineral formulas were calculated according to Lindsley and Andersen (1983; Table 3). In individual roof-zone dikes, spot analyses of clinopyroxene and orthopyroxene show a narrow compositional range with regard to quadrilateral components(~1–4%). Intracrystalline compositional ranges of quadrilateral components are as much as 10% among pyroxene from coarse-grained plutonic rocks. This larger variation appears to be an effect of the larger exsolution lamellae typical of the coarse-grained samples. However, the overall compositional trends discussed below suggest that the averages are representative of bulk pyroxene compositions.

TABLE 3—*Continued*

Clinopyroxene			
111	100	236A	645A
Compositions in wt%			
51.83	52.41	50.99	51.09
0.58	0.29	0.72	0.25
1.98	2.42	2.84	2.26
0.30	0.15	0.31	0.30
10.97	6.71	12.14	12.02
14.25	15.66	13.85	12.81
20.05	20.75	18.57	20.84
0.36	0.32	0.37	0.38
0.09	0.25	0.07	0.07
100.43	98.96	99.75	100.11
Cations per six oxygens*			
1.929	1.947	1.914	1.918
0.017	0.008	0.020	0.007
0.070	0.053	0.086	0.082
0.017	0.053	0.040	0.018
0.009	0.005	0.010	0.010
0.300	0.203	0.351	0.302
0.042	0.006	0.030	0.076
0.790	0.867	0.774	0.721
0.799	0.826	0.746	0.837
0.026	0.023	0.027	0.028
0.003	0.007	0.002	0.002
4.001	3.997	4.000	4.000

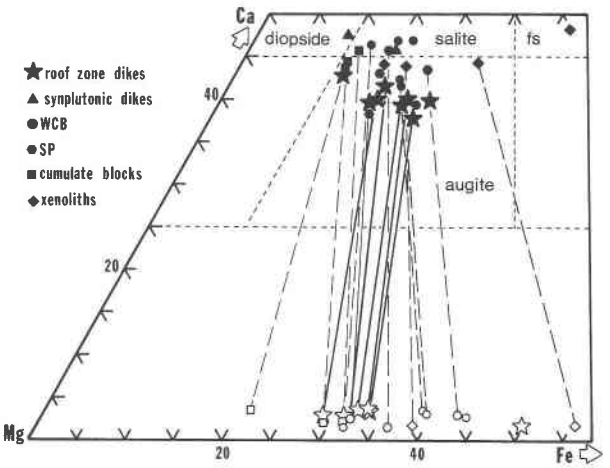

Fig. 3. Average pyroxene compositions plotted in part of the Ca-Mg-Fe ternary; fs, ferrosalite. Coexisting pyroxenes from roof-zone dikes connected by solid heavy tie lines; those from coarse-grained WCB-SP connected by dashed lines.

Nonquadrilateral components in clinopyroxene range from 2.3 to 11.1 mol% and typically total less than 9 mol%. Of the nonquadrilateral cations, Al is the most abundant, followed by Fe^{3+}, Na, Ti, Mn, and Cr (Table 3). A broad negative correlation exists between Ca and Al in clinopyroxene from the WCB-SP. In general, roof-zone dike clinopyroxene contains less Ca and a similar or greater amount of Al than clinopyroxene from the WCB, SP, synplutonic mafic dikes, and xenoliths. Clinopyroxene from orthopyroxene-free roof-zone dikes tends to be richer in Al than is clinopyroxene from two-pyroxene-bearing dikes.

The range of nonquadrilateral components in orthopyroxene is 3.3 to 6.1 mol%. Al is most abundant, followed by Mn, Fe^{3+}, Ti, Na, and Cr. Low abundances of these constituents in both clinopyroxene and orthopyroxene are typical of arc-related magmatism (e.g., Gill, 1981).

The lower Ca content of clinopyroxene from roof-zone dikes relative to that of clinopyroxene from the subjacent pluton is also easily seen in Figure 3. Orthopyroxene from roof-zone dikes is slightly richer in Ca than is orthopyroxene from the coarse-grained plutonic samples. Furthermore, tie lines between coexisting pyroxenes from the roof-zone dikes are not parallel to tie lines for the plutonic pyroxenes. The difference in Ca contents between roof-zone and plutonic pyroxenes is readily explained as a result of slower cooling and lower-temperature equilibration of the coarse-grained rocks (e.g., Lindsley and Andersen, 1983; Lindsley, 1983).

The Mg-Fe partition coefficient (K_D) for the plutonic rocks is approximately 0.54, a value shown by Kretz (1961, 1982) to be typical of granulite-facies rocks. The K_D for pyroxenes from roof-zone dikes is approximately 0.80, similar to values Kretz (1961) considered to be typical of volcanic rocks. Mg/(Mg + Fe) for roof-zone clinopyroxene is similar to that for plutonic clinopyroxene,

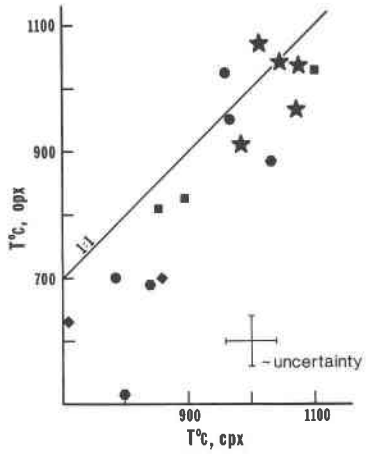

Fig. 4. Comparison of temperature estimated from orthopyroxene and clinopyroxene compositions using the geothermometer of Lindsley and Andersen (1983). Symbols as in Figure 3.

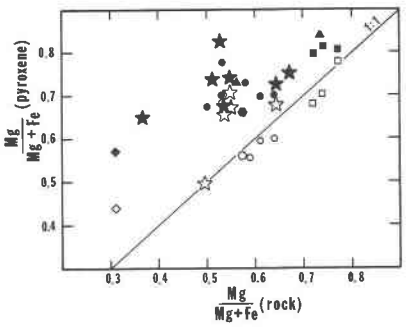

Fig. 5. Variation in pyroxene vs. whole-rock Mg/(Mg + Fe_{tot}) (atomic). Note nonregular variation of Mg/(Mg + Fe_{tot}) in roof-zone dikes and some clinopyroxene from coarse-grained samples. Symbols as in Figure 3.

but roof-zone orthopyroxene is relatively more Fe-rich than plutonic orthopyroxene. This suggests that slow cooling of the plutonic rocks lowered Mg/(Mg + Fe) in the orthopyroxene more strongly than the clinopyroxene, resulting in rotation of tie lines (Fig. 3) and a lowered K_D (Fig. 5).

Effect of pressure. One of the goals of this study was to evaluate the effect of pressure on mineral composition. The most straightforward way to estimate P_{total} of crystallization at various points in the plutonic system is to assume that the system was tilted as a coherent block. Although this assumption is quite simplistic, considerable efforts to find other useful contact metamorphic assemblages or major structural dislocations in the pluton were not successful. [Apparent retrograde assemblages in pelitic xenolith sample 219D (App. 1) support the pressure estimates made on the basis of contact metamorphic assemblages.] Figure 2 shows the estimated position of southwest-dipping isobaric surfaces in the Wooley Creek batholith that were drawn using the contact metamorphic data (also see Barnes, 1982). Owing to a lack of diagnostic contact metamorphic assemblages adjacent to the Slinkard pluton, P_{total} was estimated at 7 kbar. This estimate is consistent with regional geologic constraints and with estimated pressures of regional metamorphism to the north (Grover, 1984; Lieberman, 1983), but is considered much less certain than pressure estimates for the Wooley Creek batholith.

The Al content of clinopyroxene for the plutonic samples is broadly correlated with pressure. Clinopyroxene from the Slinkard pluton and lower Wooley Creek batholith contains an average of about 0.9 Al cations per six oxygens whereas Wooley Creek batholith roof-zone clinopyroxene contains less than 0.4 Al cations per six oxygens. The Al content of clinopyroxene from roof-zone dikes overlaps the range of Al contents in the deepest parts of the system. If one assumes that Al content and pressure are correlated and that the Al content of plutonic clinopyroxene was not reset by slow cooling, then the data suggest that the clinopyroxene-bearing roof-zone dikes are similar in bulk composition and/or depth of origin to the deepest parts of the WCB-SP.

Temperature estimates. Temperatures of pyroxene crystallization were estimated using the the two-pyroxene solvus presented by Lindsley and Andersen (1983) and Lindsley (1983). Samples in which only one pyroxene is present yield a minimum temperature estimate. Inasmuch as the equilibrium pressure of the dikes is unknown, pressure was assumed to be 5 kbar for all samples. Lindsley (1983) stated that the effect of nonquadrilateral components is to increase the uncertainty of the geothermometer and that samples with greater than 10% nonquadrilateral components should not be used. Clinopyroxenes from two samples slightly exceed this limit (samples 236A and 555, Table 3) but yield consistent temperature estimates.

With the exception of samples that show clear petrographic evidence of low-temperature equilibration, the roof-zone dike pyroxenes have average equilibrium temperatures of >910°C. Among two-pyroxene dikes, clinopyroxene temperatures range from 960°C to 1120°C and orthopyroxene temperatures range from 910°C to 1075°C (Fig. 4). One olivine- and clinopyroxene-phyric basaltic dike yielded a minimum estimated temperature of 1085°C and a clinopyroxene + hornblende andesite dike gave a minimum estimated temperature of 960°C. Relict orthopyroxene from an orthopyroxene + biotite + hornblende dacite yielded a minimum temperature estimate of 610°C.

Clinopyroxene and orthopyroxene from plutonic samples give a range of average temperature estimates from 600°C to 1030°C (Fig. 4). The lowest temperature estimates come from xenoliths and from gabbroic rocks that show chemical and petrographic evidence of crystal accumulation (Barnes, 1983). Clinopyroxene from these samples typically yields higher estimated temperatures than does orthopyroxene, providing additional evidence that plutonic orthopyroxene underwent a greater degree

of low-temperature resetting than plutonic clinopyroxene.

Relationship to whole-rock composition. Tie lines between coexisting plutonic pyroxenes in Figure 3 do not progress uniformly to higher whole-rock SiO_2 from left to right as would be expected in a calc-alkaline suite. This lack of coherence with whole-rock SiO_2 is probably a reflection of varying amounts of crystal accumulation (Barnes, 1983). Figure 5 shows that Mg/(Mg + Fe) in the plutonic pyroxenes is fairly well correlated with Mg/(Mg + Fe) in the rock. However, Mg/(Mg + Fe) in clinopyroxene in roof-zone dikes is not well correlated with Mg/(Mg + Fe) in the host (Fig. 5). Such variation among roof-zone clinopyroxene could be the result of increased f_{O_2}, increased f_{H_2O}, magma mixing, or some combination of these factors and is discussed below.

Amphibole

Amphibole is present in nearly every rock type in the WCB-SP system. Exceptions include some of the basal biotite + two-pyroxene gabbros of the Slinkard pluton, the two-mica granite and granodiorite of the Slinkard pluton, and rare biotite + two-pyroxene quartz diorite in the Wooley Creek batholith. In the lowest part of the Slinkard pluton, amphibole occurs as rims on pyroxene and as subhedral to anhedral grains in hornblende gabbro. With decreasing depth in the Slinkard pluton, subhedral hornblende is predominant. Similar upward changes in morphology are present in the Wooley Creek batholith. In the tonalitic and more felsic Wooley Creek batholith rocks, euhedral hornblende is typical (Barnes, 1983). Amphibole in roof-zone dikes occurs as hornblende rims around pyroxene or actinolitic replacement of pyroxene and as euhedral hornblende phenocrysts in samples of dacite and late-stage pyroxene + hornblende andesite dikes (Barnes et al., 1986a).

Amphibole is ubiquitous in synplutonic dikes and mafic microgranitoid enclaves and is common in mafic (metavolcaniclastic ?) xenoliths (App. 1). Some xenoliths contain both calcic amphibole and cummingtonite (App. 1).

Representative amphibole analyses are given in Table 4. In view of the interest in relating mineral composition to pressure, the site occupancy was calculated using the method outlined by Hammarstrom (1984) (all Fe as Fe^{2+}) so that the WCB-SP data could be compared to the results of Hammarstrom and Zen (1986). The data in Figures 6 and 7 were plotted using Hammarstrom's (1984) method to make such comparison possible. Site occupancy was also calculated according to the method of Robinson et al. (1982) using the program RECAMP (Spear and Kimball, 1984). For the discussion below, both methods of calculation yield similar results. The compositional variation within single amphibole grains, which is quite large in some WCB-SP samples, made it inappropriate to present average analyses. As a result, data for individual samples are shown graphically in Figures 6 and 7 as compositional ranges or, where appropriate, linear trends (fitted by eye).

Compositional variation. Numerous binary plots were generated to test interrelations among various amphibole compositional parameters. Two of these are shown in Figures 6 and 7; however, the discussion that follows will also refer to others that are not shown. As noted above, intracrystalline zoning is locally pronounced. In many cases, zoning appears to be patchy or oscillatory. (Note that no linear traverses were done; these conclusions are based on stepwise spot analyses of as many as 10 spots per grain.) Euhedral hornblende in the central to uppermost parts of the Wooley Creek batholith and in the dacitic to andesitic roof-zone dikes typically shows an overall core-to-rim decrease in ^{IV}Al and Ti, with very slight or no decrease in Mg/(Mg + Fe). Internal reversals (i.e., outward increase in Ti and ^{IV}Al) are common but are not consistent from grain to grain within a sample.

Most WCB-SP amphiboles are magnesio-hornblende (Hawthorne, 1981) and the compositional range of all nonxenolith amphibole is from tschermakitic hornblende to actinolite (Fig. 6). Calcic amphibole in xenoliths ranges from ferro-tschermakitic hornblende in sample 7B and ferroan pargasitic hornblende in 219B, to ferro-hornblende in sample 219A, and magnesio-hornblende and actinolitic hornblende in sample 119 (Fig. 6C). Cummingtonite is present in two of the most Fe-rich xenoliths and has a slightly higher Mg/(Mg + Fe) than coexisting ferro-hornblende.

WCB-SP hornblende spans a wide range of Mg/(Mg + Fe) that is generally correlative with the range of whole-rock Mg/(Mg + Fe). In Figure 6A, hornblende from the Wooley Creek batholith is divided into three groups on the basis of Mg/(Mg + Fe). These groups correspond to compositional divisions recognized by Barnes et al. (1986a) and Barnes (1983): a pyroxene-bearing group (group 1), an intermediate (biotite + hornblende + pyroxene)–bearing group (group 2), and a (biotite + hornblende)–bearing group in which only the most mafic samples have chemical and petrographic evidence for primary pyroxene (group 3). Figure 6A shows that hornblende from the Slinkard pluton and groups 1 and 2 has higher Mg/(Mg + Fe) than hornblende from group 3 or from the roof-zone dikes. The single exception to this upward decrease in Mg/(Mg + Fe) is sample 377 from the late-stage stock in the southern Wooley Creek batholith (Fig. 2). Hornblende from this sample is considerably more magnesian than hornblende from other samples with similar whole-rock SiO_2 content.

Considerable interest has been shown in the apparent genetic relationship between mafic synplutonic dikes and mafic microgranitoid enclaves (Didier, 1973; Vernon, 1983; Reid et al., 1983; Barnes, 1983; Furman and Spera, 1984; Bussell, 1985; Barnes et al., 1986a). Reid and Hamilton (1985) suggested that comparing amphibole compositions from mafic microgranitoid enclaves and from their host pluton can provide insight into the origin of the enclaves. In order to determine the range of compositions among mafic synplutonic dikes, hornblende was analyzed in several dike samples and one sample of host

TABLE 4. Representative amphibole analyses

	548-2			579-3		697-2		397-2	317-1	
	Core	Rim	Gm.*	Core	Rim	Core	Rim	Core	Core	Rim
					Compositions in wt%					
SiO_2	45.68	49.28	46.40	48.65	49.52	47.03	49.54	46.17	45.31	45.42
Al_2O_3	8.01	5.09	7.73	5.02	4.87	7.48	5.09	7.77	8.84	8.58
FeO	17.07	17.35	17.36	18.18	18.12	16.78	17.41	15.27	17.11	16.90
MgO	11.45	12.22	11.76	11.91	11.89	11.88	12.39	12.41	11.54	11.19
TiO_2	1.65	1.04	1.02	0.61	0.51	1.34	0.71	1.57	1.50	1.01
MnO	0.39	0.41	0.43	0.57	0.50	0.45	0.49	0.30	0.38	0.42
CaO	10.49	10.82	10.37	10.97	10.98	11.18	11.15	11.68	10.91	11.44
Na_2O	1.58	0.84	1.45	0.88	0.80	1.22	0.92	1.20	1.58	1.21
K_2O	0.73	0.46	0.50	0.41	0.38	0.51	0.35	0.73	0.73	0.80
Total	97.05	97.51	97.02	97.22	97.56	97.87	98.04	97.11	97.90	96.97
					Cations per 23 oxygens**					
Si	6.871	7.269	6.964	7.220	7.318	6.983	7.258	6.888	6.766	6.832
^{IV}Al	1.129	0.731	1.036	0.780	0.682	1.017	0.742	1.112	1.234	1.168
Al_{tot}	1.420	0.885	1.368	0.878	0.848	1.309	0.879	1.367	1.556	1.522
^{VI}Al	0.291	0.155	0.332	0.098	0.166	0.292	0.137	0.254	0.322	0.354
Ti	0.187	0.115	0.115	0.068	0.057	0.150	0.078	0.176	0.168	0.114
Fe^{3+}	0.000	0.302	0.000	0.468	0.339	0.000	0.390	0.019	0.000	0.079
Mg	2.567	2.686	2.630	2.634	2.618	2.629	2.705	2.759	2.568	2.509
Fe^{2+}	2.147	1.838	2.179	1.789	1.900	2.084	1.744	1.886	2.137	2.047
Mn	0.050	0.051	0.055	0.072	0.063	0.057	0.061	0.038	0.048	0.054
Sum (M1–M3)	13.241	13.148	13.311	13.129	13.143	13.211	13.115	13.133	13.244	13.156
Ca	1.691	1.710	1.668	1.744	1.739	1.779	1.750	1.867	1.746	1.844
Na (M4)	0.068	0.142	0.022	0.127	0.119	0.011	0.134	0.000	0.011	0.000
Na_{tot}	0.461	0.24	0.422	0.253	0.229	0.351	0.261	0.347	0.457	0.353
Na (A)	0.393	0.098	0.4	0.127	0.111	0.340	0.127	0.347	0.447	0.353
K	0.140	0.087	0.096	0.078	0.072	0.097	0.065	0.139	0.139	0.154
Total	15.533	15.185	15.497	15.204	15.183	15.438	15.191	15.486	15.586	15.507

* Groundmass.
** Site occupancy estimated according to Spear and Kimball (1984) using average Fe^{3+}.

rock collected in a small well-exposed cirque basin (Cuddihy Lakes, Fig. 2). In addition, hornblende was analyzed in host-enclave pairs from two other localities. Figures 6B and 6C show a wide range of Mg/(Mg + Fe) among the mafic synplutonic dikes but a narrow range among the enclave-host pairs. Note that the compositional fields for enclaves 686B and 686E are not precisely correlative with the field for the host (687); however, there is complete overlap among enclave 681B and its host 681Ah.

Among individual samples, total Na cations commonly show a broad positive correlation with ^{IV}Al. Samples from the structurally lowest part of the system (Slinkard pluton and group 1) contain the least Na at a given ^{IV}Al content, roof-zone dike and group 3 samples contain the most Na, and group 2 samples are intermediate with broad overlap.

Robinson et al. (1971) showed that substitution of Al for Si in tetrahedral sites can be accommodated by substitutions of Na^+ and K^+ in the A site and Al^{3+}, Fe^{3+}, and Ti^{4+} in octahedral sites. This leads to the relationship ^{IV}Al = A-site cations + $^{VI}Al^{3+}$ + $^{VI}Fe^{3+}$ + $2Ti^{4+}$. Solid solution among the WCB-SP amphiboles is well represented by this set of substitutions, as are amphiboles in mafic synplutonic dikes and mafic microgranitoid enclaves.

Edenite-type substitution of Na^+ and K^+ in the A site and ^{IV}Al for Si in the tetrahedral sites (with Na in M4 subtracted to account for richterite-type substitution) can account for some, but certainly not all, ^{IV}Al in WCB-SP hornblende.

Hammarstrom (1984) and Hammarstrom and Zen (1986) suggested that total Al content of hornblende in equilibrium with quartz is a function of pressure. The WCB-SP system seemed to be an ideal setting in which to test such an idea. However, two difficulties are apparent: individual samples show a wide range of total Al in primary hornblende, and in many samples (especially in groups 1, 2, some mafic microgranitoid enclaves, mafic synplutonic dikes, and roof-zone pyroxene + hornblende andesite), quartz is absent or there is no textural evidence for equilibrium among hornblende and quartz.

Figure 7A shows the range in total Al for coarse-grained rocks of the WCB-SP and for the roof-zone dikes. For a given ^{IV}Al content, total Al content shows an overall increase with increase in pressure, but the range in total Al at constant ^{IV}Al is much less than that predicted by Hammarstrom and Zen (1986) for a 3.5-kbar pressure difference. Plots of maximum total Al content and average Al content versus pressure for all samples showed no significant correlation.

Hornblende from mafic synplutonic dikes in the Cuddihy basin (Fig. 7B) show a range of total Al (at constant ^{IV}Al) almost as large as for the entire Wooley Creek batholith. Hornblende in the Cuddihy dikes is clearly not in equilibrium with hornblende in the host. Figures 7B and 7C show the range for enclave 681 and its host and

TABLE 4—*Continued*

471-1			777B-1		638-1		686B-1	686E-3	687-3	377-2	
Core	Mid	Rim	Core	Rim	Core	Rim	Core	Rim	Core	Core	Rim
					Compositions in wt%						
45.39	44.94	47.30	45.72	46.37	45.66	50.95	45.49	43.91	45.05	46.88	47.57
8.18	8.40	6.33	8.96	8.68	10.81	5.88	8.36	9.82	8.33	7.13	6.27
15.91	16.62	16.39	15.77	16.39	10.05	9.45	17.27	17.43	17.08	14.7	14.79
12.39	11.70	12.70	12.02	12.36	14.98	17.14	11.18	10.95	11.53	12.95	13.19
2.06	1.53	0.69	1.75	0.7	1.19	0.24	1.7	1.77	1.51	0.99	0.78
0.31	0.40	0.45	0.23	0.39	0.18	0.25	0.44	0.34	0.45	0.96	1.01
10.90	11.29	11.27	11.18	10.96	11.7	11.86	11.65	12.26	11.22	11.79	11.7
1.68	1.45	0.89	1.13	1.11	1.54	0.89	1.48	1.38	1.59	1.61	1.41
0.76	0.71	0.62	0.73	0.45	0.52	0.3	0.29	0.86	0.59	0.56	0.46
97.58	97.04	96.64	97.49	97.41	96.63	96.96	97.86	98.72	97.35	97.57	97.18
					Cations per 23 oxygens**						
6.772	6.757	7.069	6.795	6.864	6.668	7.318	6.802	6.512	6.766	6.958	7.067
1.228	1.243	0.931	1.205	1.136	1.332	0.682	1.198	1.488	1.234	1.042	0.933
1.439	1.489	1.115	1.570	1.515	1.861	0.996	1.433	1.717	1.475	1.248	1.098
0.210	0.246	0.184	0.365	0.379	0.529	0.314	0.235	0.229	0.241	0.205	0.165
0.231	0.173	0.078	0.196	0.078	0.131	0.026	0.191	0.197	0.171	0.110	0.087
0.000	0.093	0.216	0.000	0.150	0.009	0.013	0.096	0.304	0.076	0.047	0.100
2.755	2.622	2.829	2.662	2.727	3.260	3.669	2.491	2.420	2.581	2.864	2.920
1.985	1.997	1.832	1.960	1.879	1.218	1.122	2.064	1.858	2.069	1.777	1.738
0.039	0.051	0.057	0.029	0.049	0.022	0.030	0.056	0.043	0.057	0.121	0.127
13.220	13.181	13.195	13.212	13.262	13.169	13.175	13.133	13.052	13.194	13.125	13.138
1.742	1.819	1.805	1.780	1.738	1.831	1.825	1.867	1.948	1.806	1.875	1.862
0.037	0.000	0.000	0.008	0.000	0.000	0.000	0.000	0.000	0.000	0.000	0.000
0.486	0.423	0.258	0.326	0.319	0.436	0.248	0.429	0.397	0.463	0.463	0.406
0.449	0.423	0.258	0.318	0.319	0.436	0.248	0.429	0.397	0.463	0.463	0.406
0.145	0.136	0.118	0.138	0.132	0.097	0.055	0.055	0.163	0.113	0.106	0.087
15.593	15.559	15.376	15.456	15.451	15.533	15.303	15.484	15.560	15.576	15.569	15.493

for enclaves 686B and 686E and their host, respectively. Enclaves 686B and 686E have a larger compositional range and elevated ^{IV}Al and total Al relative to the host, whereas enclave 681 is indistinguishable from its host.

Biotite

Petrographic evidence suggests that biotite was the last ferromagnesian phase to crystallize in the WCB-SP. In most cases, biotite followed hornblende in the mafic paragenetic sequence; however, some biotite + two-pyroxene rocks are present in the lower parts of both the Wooley Creek batholith and the Slinkard pluton (App. 1). Biotite in roof-zone dikes occurs as fine-grained late-stage groundmass grains in andesitic dikes and as euhedral to subhedral phenocrysts in dacitic dikes. Euhedral hornblende is a common inclusion in biotite from roof-zone dacite dikes.

Microprobe analyses show negligible intracrystalline variation and little variation among crystals in most samples. Exceptions are samples in which biotite is an interstitial phase (e.g., samples 236A, 184).

Fe^{2+} was measured for biotite in samples 471 and 377 (Table 5). A plot representing the Fe^{3+}-, Fe^{2+}-, and Mg-bearing biotite end members (Fig. 8) shows that WCB-SP biotite is similar to biotite from the Sierra Nevada batholith (Dodge et al., 1969). These data suggest that biotite in the WCB-SP crystallized under f_{O_2} conditions between the NNO and HM buffers. Minor constituents show no correlation with Fe/(Fe + Mg). However, MnO is weakly correlated with whole-rock SiO_2 content and shows a range from 0.02 to 0.80 wt%. The highest MnO content was measured in sample 377, which has high whole-rock SiO_2 content (69.28%) but relatively low Fe/

TABLE 5. Representative biotite analyses

	377	471	642A-3	548-2	579-1
			Compositions in wt%		
SiO_2	36.61	35.67	33.83	35.22	35.55
TiO_2	2.75	3.63	1.93	4.02	3.56
Al_2O_3	13.73	13.96	18.97	13.81	14.21
Fe_2O_3	5.79	5.31	n.d.	n.d.	n.d.
FeO	11.65	15.59	24.28	19.98	20.77
MnO	0.69	0.28	0.57	0.17	0.21
MgO	13.49	11.01	4.61	11.13	10.62
CaO	0.07	0.02	0.05	0.02	0.02
Na_2O	0.06	0.16	0.05	0.08	0.09
K_2O	9.58	9.31	9.75	9.01	9.30
Total	94.42	94.94	94.05	93.45	94.34
			Cations per 22 oxygens		
Si	5.560	5.477	5.390	5.527	5.547
Ti	0.314	0.419	0.231	0.474	0.418
Al	2.459	2.527	3.563	2.555	2.615
Fe^{+3}	0.662	0.614	n.d.	n.d.	n.d.
Fe^{+2}	1.480	2.002	3.253	2.622	2.710
Mn	0.089	0.036	0.077	0.023	0.028
Mg	3.054	2.520	1.095	2.603	2.470
Ca	0.011	0.003	0.009	0.003	0.003
Na	0.018	0.048	0.015	0.024	0.027
K	1.856	1.824	1.982	1.804	1.851
Total	15.503	15.470	15.597	15.635	15.668

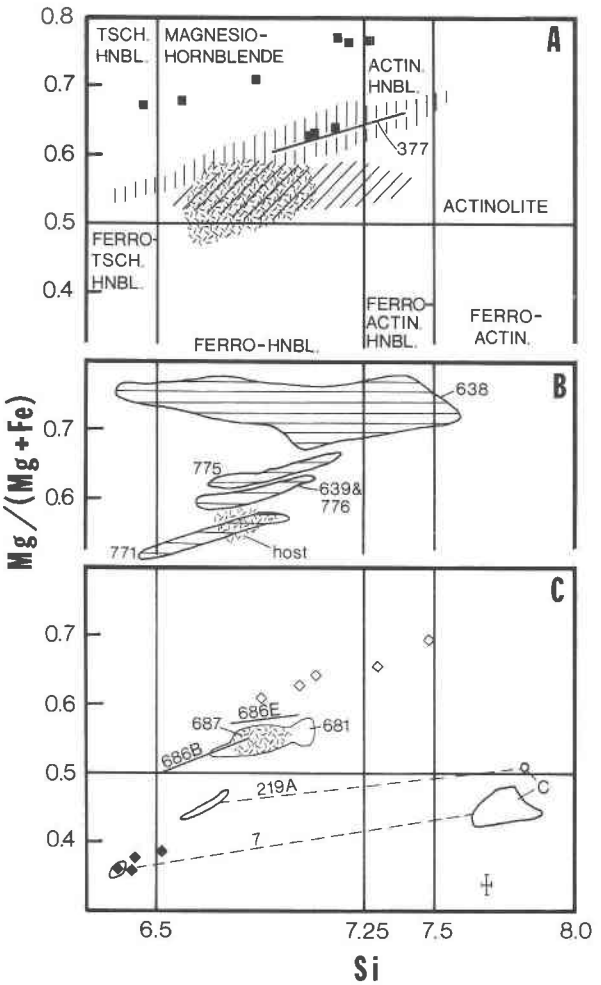

Fig. 6. Mg/(Mg + Fe_{tot}) in amphibole vs. Si cations. Classification after Hawthorne (1981). (A) Vertical ruling, range of SP and lower WCB (groups 1 and 2); inclined ruling, roof-zone dikes; patterned area, upper WCB (group 3). Line shows range of amphibole composition in late-stage granitic intrusive in upper WCB (377). Squares are spot analyses of hornblende from cumulate blocks. (B) Horizontal ruling, range of hornblende composition in synplutonic mafic dikes; patterned area, composition of hornblende in plutonic host to dikes. (C) Lines, range in hornblende composition in mafic microgranitoid enclaves 686B and 686E; patterned area, range of granodioritic host 687. Enclosed area labeled 681 gives range of hornblende in enclave and host samples. Filled diamonds, xenolith 219B; unfilled diamonds, xenolith 119. Fields connected by dashed lines indicate xenoliths 7 and 219A with coexisting calcic amphibole and cummingtonite (c).

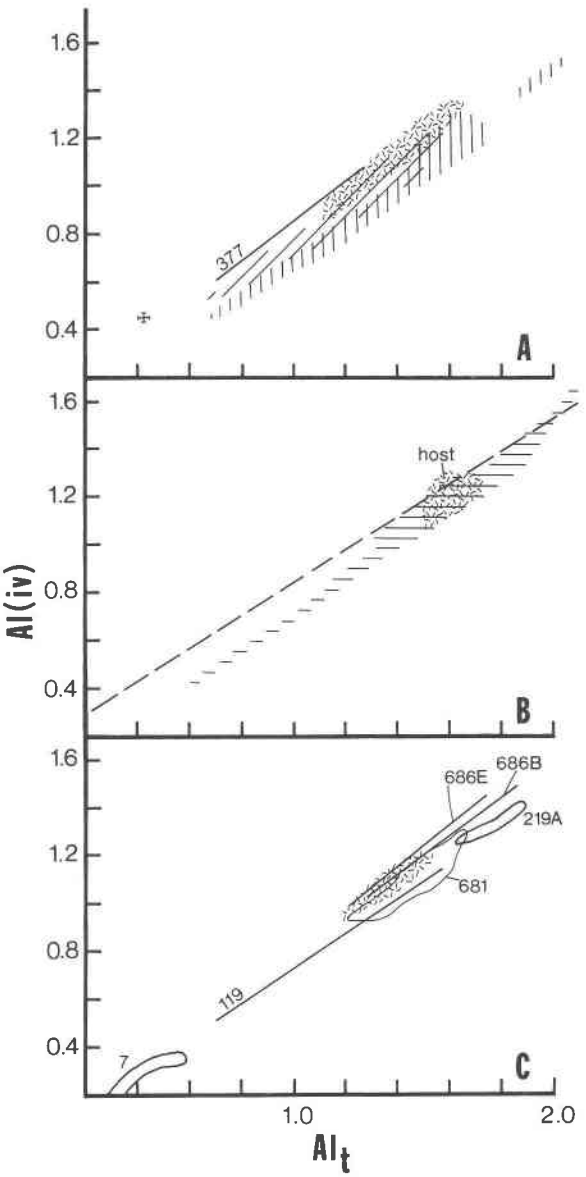

Fig. 7. Total Al vs. ^{IV}Al (cations) in amphibole. Symbols as in Figure 6. Dashed line in (B) represents relation between ^{IV}Al and Al_{total} determined by Hammarstrom and Zen (1986).

(Fe + Mg) (~0.41). ^{VI}Al content is low (<0.3 cations per 22 oxygens) in all samples of magmatic biotite except for sample 642A, the two-mica granite of the Slinkard pluton (Table 5, Fig. 2), which contains 0.84 ^{VI}Al cations. Metasedimentary xenolith samples 219A and 219D contain biotite with 0.034 and 0.058 ^{VI}Al cations, respectively. F was measured in two samples (471 and 548) and is low in both (0.1 to 0.2 wt%).

Hornblende and biotite variation vs. whole-rock composition

Hornblende and biotite show good correlation with whole-rock Fe/(Fe + Mg) except for the late-stage stock in the southern Wooley Creek batholith (sample 377), in which hornblende and biotite are considerably more magnesian than expected. Figure 9 shows the lack of correlation among mineral Fe/(Fe + Mg) and whole-rock SiO_2 contents. In general, Fe/(Fe + Mg) in biotite is greater than Fe/(Fe + Mg) in hornblende in a given sample. Among group 3 samples, Fe/(Fe + Mg) in hornblende is nearly constant at a value of ~0.45. With the exception of sample 377 (late-stage stock in the southern Wooley

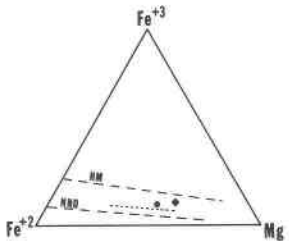

Fig. 8. Ternary diagram of biotite composition in terms of Mg-, Fe^{2+}-, and Fe^{3+}-bearing end members. Dot, WCB granodiorite 471; diamond, late-stage WCB granite 377. Long-dashed curves represent HM and NNO buffers; short-dashed curve represents Sierra Nevada biotite (Dodge et al., 1969).

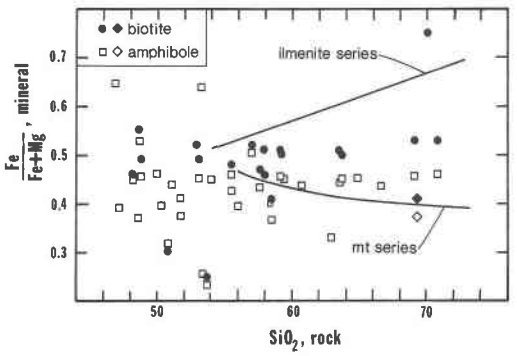

Fig. 9. Cationic Fe/(Fe + Mg) in biotite and amphibole vs. whole-rock SiO_2 content. Diamonds are for late-stage granite sample 377. Trends for ilmenite and magnetite series are for the Takanawa and Daito-Yokota suites, respectively, of the central Chugoku granitoids (Czamanske et al., 1981).

Creek batholith), all group 3 samples contain biotite in which Fe/(Fe + Mg) is between 0.5 and 0.55 (Fig. 9). Biotite from groups 1 and 2, from mafic synplutonic dikes, and from xenoliths shows a wide range of Fe/(Fe + Mg) that probably reflects whole-rock composition. The highest value of Fe/(Fe + Mg) is for the Slinkard pluton two-mica granite sample 642A. Figure 9 also shows the trends for magnetite-series and ilmenite-series biotite from a suite of Japanese granitoids (Czamanske et al., 1981). If mafic compositions and Slinkard pluton sample 642A are excluded, granitoids of the WCB-SP are approximately intermediate between the two Japanese suites. The overall lack of Fe enrichment with increasing SiO_2 shown in Figure 9 suggests that the WCB-SP magma was relatively oxidizing, in accord with f_{O_2} estimates based on biotite Fe^{3+} content.

Oxide minerals

Oxide minerals are ubiquitous but generally sparse in WCB-SP samples. Magnetite and ilmenite and their alteration products are the principal oxides, but chromite occurs as inclusions in pyroxene from cumulate gabbroic blocks (Barnes, 1983). In plutonic samples, the Fe-Ti oxides typically occur as inclusions in hornblende and rarely in biotite and plagioclase. Fe-Ti oxides are commonly present where pyroxene is rimmed by hornblende or replaced by actinolitic amphibole. Microprobe analyses show that in the plutonic samples, ilmenite is nearly pure and primary titanomagnetite has undergone the effects of slow cooling and oxyexsolution. Most commonly, original titanomagnetite is now a lamellar intergrowth of ilmenite + hematite ± goethite. The presence of goethite was surprising because many of the samples that contain ilmenite-goethite intergrowths show no other evidence of weathering. Only one of the analyzed plutonic samples lacks ilmenite as a primary phase. This is sample 377, from the late-stage stock in the southern Wooley Creek batholith. The sample is also distinctive in that relict titanomagnetite occurs as inclusions in poikilitic alkali feldspar with euhedral (primary) titanite and zircon. This is the only sample in the WCB-SP system in which titanite is a primary phase.

Relict magnetite is present (with pyrite and pyrrhotite) in several of the analyzed metasedimentary xenoliths. Ilmenite is the only oxide phase in metasedimentary xenoliths 133 and metavolcanic xenoliths 119 and 179 (App. 1).

Magnetite and ilmenite in the roof-zone dikes occur as small (~50-μm diameter) inclusions in pyroxene and plagioclase, as microphenocryst and groundmass crystals, and as grains associated with reaction of pyroxene to actinolitic amphibole. As with the pyroxenes, the Fe-Ti oxides in the roof-zone dikes seemed the most likely to retain magmatic compositions. All titanomagnetite shows oxyexsolution features that range from sandwich through composite to trellis intergrowths (see Haggerty, 1976a). In general, lamellae are less than 2 μm wide. Ilmenite typically occurs as composite grains of ilmenite and "exsolved" titanomagnetite. Because of the thin lamellae in magnetite, it was not possible to determine a primary composition by integration of host and lamellae compositions. Therefore, analyses in Table 6 represent an average of several spot analyses. Mineral formulas were calculated using the method of Stormer (1983).

Titanomagnetite from the roof-zone dikes ranges in composition from X_{usp} (mole fraction ulvöspinel) 0.31 to 0.56. The lowest values are from inclusions in clinopyroxene (in general from 0.31 to 0.39) whereas the highest are from inclusions in plagioclase phenocrysts (0.42 to 0.53) and groundmass crystals (0.38 to 0.51). The highest X_{usp} value (0.56) is from an inclusion that lies on a prominent crack in the host clinopyroxene crystal. Ilmenite compositions (X_{ilm}) range from 0.89 to 0.99 (Table 6).

Fe-Ti oxide geothermometry and oxygen barometry. The difficulties in extracting magmatic temperature and f_{O_2} from compositions of slowly cooled Fe-Ti oxides are well known. In view of the common late-stage alteration to hematite in the plutonic samples, such estimates were not attempted. It was thought that temperature-f_{O_2} data could be retrieved from compositions of oxides in the roof-zone dikes; however, the wide range in X_{usp} among groundmass titanomagnetite and titanomagnetite inclusions in clino-

TABLE 6. Representative magnetite analyses

	553-1	555-3	699-1	699-2	704-1
	Compositions in wt%				
SiO_2	0.08	0.16	0.11	0.07	0.13
TiO_2	13.11	11.39	18.98	12.82	12.84
Al_2O_3	0.06	3.90	0.13	0.17	0.00
Cr_2O_3	1.70	0.52	0.13	0.08	0.00
FeO	79.29	78.00	76.51	81.38	77.74
MnO	1.02	0.69	0.98	0.86	0.43
MgO	0.04	0.45	0.07	0.04	2.02
Total	95.29	95.11	96.90	95.42	93.16
	Cations per four oxygens*				
Si	0.002	0.005	0.003	0.002	0.005
Ti	0.377	0.320	0.538	0.367	0.370
Al	0.002	0.171	0.006	0.006	0.000
Cr	0.050	0.014	0.003	0.002	0.000
Fe^{3+}	1.190	1.164	0.907	1.253	1.251
Fe^{2+}	1.344	1.279	1.508	1.341	1.240
Mn	0.032	0.021	0.031	0.027	0.014
Mg	0.001	0.025	0.003	0.001	0.115
Total	3.000	3.000	3.000	3.000	3.000
X_{usp}	0.39	0.38	0.54	0.37	0.35

* Calculated according to Stormer (1983).

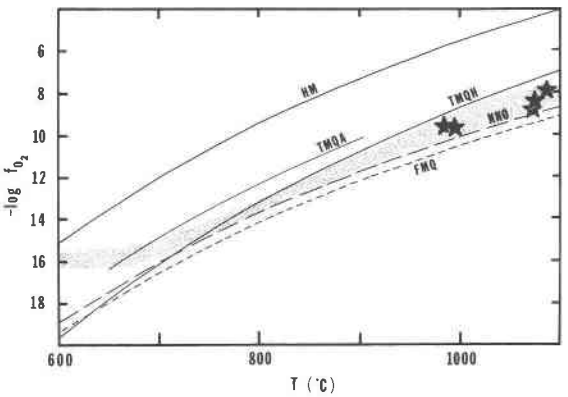

Fig. 10. Estimated T-f_{O_2} conditions for the WCB-SP. Buffer curves for fayalite + magnetite + quartz (FMQ; Hewitt, 1978), Ni-NiO (NNO; Huebner and Sato, 1970), hematite + magnetite (HM; Chou, 1978), titanite + magnetite + ilmenite + quartz + hedenbergite (TMQH; Wones, 1981), and titanite + magnetite + ilmenite + quartz + amphibole (TMQA; Noyes et al., 1983). All buffer curves plotted assuming pure phases. Stars are for roof-zone dikes. See text for further explanation.

pyroxene (in a single sample) indicates that significant low-temperature equilibration occurred in the dike rocks as well. Uncritical application of the temperature-f_{O_2} grid (Spencer and Lindsley, 1981) resulted in a temperature range from <700°C to 1100°C and f_{O_2} conditions from above NNO to one log unit below FMQ. The low f_{O_2} estimates are primarily due to the high X_{ilm} in composite ilmenite grains and suggest that all of the ilmenite analyzed has undergone oxidation and re-equilibration.

In an attempt to salvage some information from the oxide data, the integrated compositions of titanomagnetite *inclusions in clinopyroxene* were assumed to represent primary compositions. Equilibrium temperature was assumed to be that estimated from two-pyroxene geothermometry (see above). If the clinopyroxene host, titanomagnetite, and a rhombohedral oxide phase were in equilibrium, as suggested by petrographic data, then f_{O_2} can be estimated using the two-pyroxene temperature, X_{usp}, and the data of Spencer and Lindsley (1981). The results of these estimates are plotted in Figure 10 and show oxygen fugacity to have been slightly above the NNO buffer. These results are in accord with oxygen fugacities estimated from biotite compositions (see above) and are typical of calc-alkaline magmas (e.g., Haggerty, 1976b). The uncertainty in f_{O_2} based solely on temperature uncertainties (~80°C) is on the order of 1.5 log units.

TABLE 7. Representative plagioclase analyses

	704-3			557-2			555-1		548-3		697-2		
	Core	Mid	Rim	Core	Mid	Rim	Core	Rim	Core	Rim	Core	Mid	Rim
	Compositions in wt%												
SiO_2	53.22	55.38	54.77	52.93	54.82	53.22	45.88	49.96	55.28	58.60	58.25	55.57	60.05
Al_2O_3	29.46	28.36	28.48	29.53	28.31	29.29	34.70	32.50	28.57	26.61	26.48	27.73	25.16
FeO	0.58	0.45	0.59	0.53	0.58	0.59	0.25	0.23	0.18	0.07	0.10	0.09	0.06
CaO	12.02	10.76	11.15	12.60	11.14	12.38	17.43	14.95	10.64	8.16	8.04	9.72	6.28
Na_2O	4.43	5.18	4.95	4.09	4.71	4.35	1.33	2.94	5.20	6.64	6.77	5.77	7.88
K_2O	0.30	0.38	0.34	0.33	0.41	0.32	0.04	0.07	0.21	0.22	0.29	0.21	0.33
TiO_2	0.07	0.04	0.05	0.09	0.04	0.14	0.10	0.03	0.00	0.00	0.00	0.00	0.00
SrO	0.02	0.31	0.10	0.00	0.05	0.08	0.16	0.00	0.32	0.30	0.27	0.30	0.25
Total	100.09	100.86	100.43	100.10	100.08	100.38	99.89	100.68	100.46	100.62	100.21	99.38	100.01
	Cations per eight oxygens												
Si	2.413	2.482	2.468	2.401	2.476	2.410	2.113	2.264	2.484	2.607	2.603	2.517	2.677
Al	1.573	1.498	1.511	1.579	1.507	1.563	1.883	1.736	1.512	1.394	1.394	1.479	1.321
Fe	0.021	0.016	0.021	0.020	0.021	0.021	0.009	0.008	0.006	0.002	0.002	0.002	0.001
Ca	0.583	0.517	0.538	0.612	0.538	0.600	0.860	0.725	0.511	0.389	0.384	0.472	0.299
Na	0.388	0.450	0.432	0.359	0.412	0.381	0.119	0.258	0.452	0.572	0.586	0.506	0.680
K	0.017	0.021	0.018	0.019	0.022	0.017	0.001	0.004	0.012	0.012	0.016	0.012	0.018
Ti	0.001	0.001	0.001	0.002	0.001	0.004	0.002	0.000	0.000	0.000	0.000	0.000	0.000
Sr	0.000	0.008	0.001	0.000	0.001	0.001	0.004	0.000	0.008	0.006	0.006	0.008	0.006
Total	4.996	4.992	4.990	4.992	4.978	4.997	4.992	4.994	4.985	4.982	4.991	4.996	5.003

Muscovite

Muscovite with primary textural features (Miller et al., 1981) occurs only in the two-mica granite of the Slinkard pluton (sample 642A). Relative to muscovite interpreted as primary by Miller et al. (1981), muscovite from the Slinkard pluton has lower Fe and Ti, slightly lower Mg, and higher Na and Al. These compositional features appear to be compatible with a primary origin. Sample 642A also contains aluminous biotite (Table 5) and almandine-spessartine garnet (App. 1), as is typical of peraluminous granitoids in which muscovite is a primary phase.

Plagioclase

Figure 11A shows the range in plagioclase compositions of the roof-zone dikes. The roof-zone dikes are divided into those that intruded prior to emplacement of the uppermost granodiorite of the Wooley Creek batholith and those that followed grandiorite emplacement (see Barnes et al., 1986a). Plagioclase phenocrysts in the most mafic roof-zone dikes range from An_{88} to An_{71} (Table 7) and show normal zoning. Plagioclase phenocrysts in pregranodiorite two-pyroxene andesite range from An_{67} to An_{51}. Both oscillatory-normal and oscillatory-reverse zoning was observed in individual samples (Fig. 11A). Postgranodiorite two-pyroxene andesites have similar zoning patterns but show a wider range of compositions, from An_{77} to An_{50}. Pregranodiorite dacitic dikes have predominantly oscillatory-normal zoning, from An_{53} to An_{29}. Late-stage evolved dikes include pyroxene + hornblende andesite (693) and biotite + hornblende dacite (579 and 697). As with the postgranodiorite two-pyroxene andesites, compositional reversals are common, and both oscillatory-normal and oscillatory-reverse zoned phenocrysts are present in individual samples. Plagioclase from these late-stage dikes has the widest compositional range of any of the roof-zone dike groups (An_{58} to An_{28}) but has core compositions similar to plagioclase phenocrysts in the pregranodiorite dacitic dikes (Fig. 11A).

Cumulate gabbroic blocks from the Wooley Creek batholith have interstitial plagioclase that shows a wide range of compositions, from An_{74} to An_{43} (Fig. 11B). Two samples of mafic selvages in the roof-zone (236A and 257A) show distinctive plagioclase compositions. Porphyritic sample 236A has a range of plagioclase compositions similar to the gabbroic blocks. However, plagioclase from a coarse-grained selvage of hornblende + two-pyroxene gabbro shows reverse zoning from An_{91} to An_{81}, the most calcic plagioclase in the system.

Group 1 plagioclase (Fig. 11B) ranges from An_{65} to An_{36}. Zoning is weak in many samples and is normal to oscillatory-normal. The weakest zoning occurs in strongly foliated samples in which bent plagioclase crystals are common. Among group 1 samples, there is no correlation between plagioclase composition and whole-rock MgO or SiO_2 or between plagioclase composition and estimated pressure. Group 2 samples have plagioclase compositions similar to the most Ca-rich plagioclase of group 1. Individual group 2 samples show both oscillatory-normal and oscillatory-reverse crystals. Group 3 plagioclase ranges from weakly zoned (An_{46} to An_{42}) to strongly normally zoned (e.g., An_{31} to An_{12}; Fig. 11B). There is a general correlation between plagioclase composition and whole-rock SiO_2 content in group 3 samples.

Plagioclase compositions from mafic synplutonic dikes and from their host quartz diorite are shown in Figure 11C. Most dike plagioclase is weakly zoned and is virtually identical in composition to plagioclase in the host. An-rich plagioclase is present in three samples, but only one of these (776) is not predominantly andesine bearing. The sodic plagioclase in sample 638 is interstitial among

TABLE 7—*Continued*

377-1		642A-1		687-3			639		638	686B		775A	
Core	Rim	Core	Rim	Core	Mid	Rim	gmA	gmB	Avg.	Core	Rim	Core	Rim
Compositions in wt%													
60.05	65.36	60.60	64.12	55.73	55.66	59.03	50.27	56.08	58.88	48.36	56.33	48.57	54.20
24.56	21.29	24.29	22.55	27.69	27.82	25.25	31.56	28.02	25.88	32.94	27.71	32.93	28.89
0.11	0.21	0.00	0.04	0.17	0.19	0.14	0.12	0.10	0.05	0.14	0.05	0.11	0.04
6.09	2.25	5.75	3.65	9.66	10.04	7.09	14.42	9.95	7.86	15.82	9.46	15.43	10.67
7.60	10.07	8.00	9.43	5.68	5.60	7.43	3.04	5.56	6.90	2.35	6.07	2.49	5.10
0.33	0.37	0.27	0.17	0.21	0.20	0.28	0.07	0.07	0.33	0.08	0.10	0.02	0.06
0.00	0.00	0.00	0.00	0.00	0.00	0.00	0.00	0.00	0.00	0.00	0.04	0.00	0.00
0.41	0.25	0.30	0.21	0.31	0.27	0.29	0.28	0.29	0.11	0.22	0.00	0.00	0.04
99.16	99.79	99.20	100.16	99.45	99.77	99.50	99.75	100.06	100.01	99.90	99.77	99.55	99.01
Cations per eight oxygens													
2.699	2.886	2.716	2.825	2.522	2.512	2.653	2.296	2.518	2.631	2.216	2.532	2.226	2.463
1.301	1.108	1.282	1.170	1.477	1.479	1.337	1.698	1.482	1.363	1.779	1.458	1.779	1.547
0.004	0.007	0.000	0.001	0.005	0.006	0.005	0.004	0.002	0.001	0.004	0.001	0.004	0.001
0.292	0.106	0.276	0.172	0.467	0.484	0.341	0.705	0.478	0.376	0.776	0.455	0.757	0.519
0.662	0.861	0.694	0.805	0.498	0.488	0.646	0.268	0.483	0.598	0.208	0.527	0.220	0.449
0.018	0.021	0.014	0.009	0.012	0.010	0.016	0.004	0.004	0.018	0.004	0.005	0.000	0.002
0.000	0.000	0.000	0.000	0.000	0.000	0.000	0.000	0.000	0.000	0.000	0.001	0.000	0.000
0.010	0.005	0.006	0.005	0.008	0.006	0.006	0.006	0.006	0.002	0.005	0.000	0.000	0.000
4.987	4.994	4.989	4.987	4.988	4.987	5.004	4.981	4.975	4.989	4.993	4.989	4.986	4.981

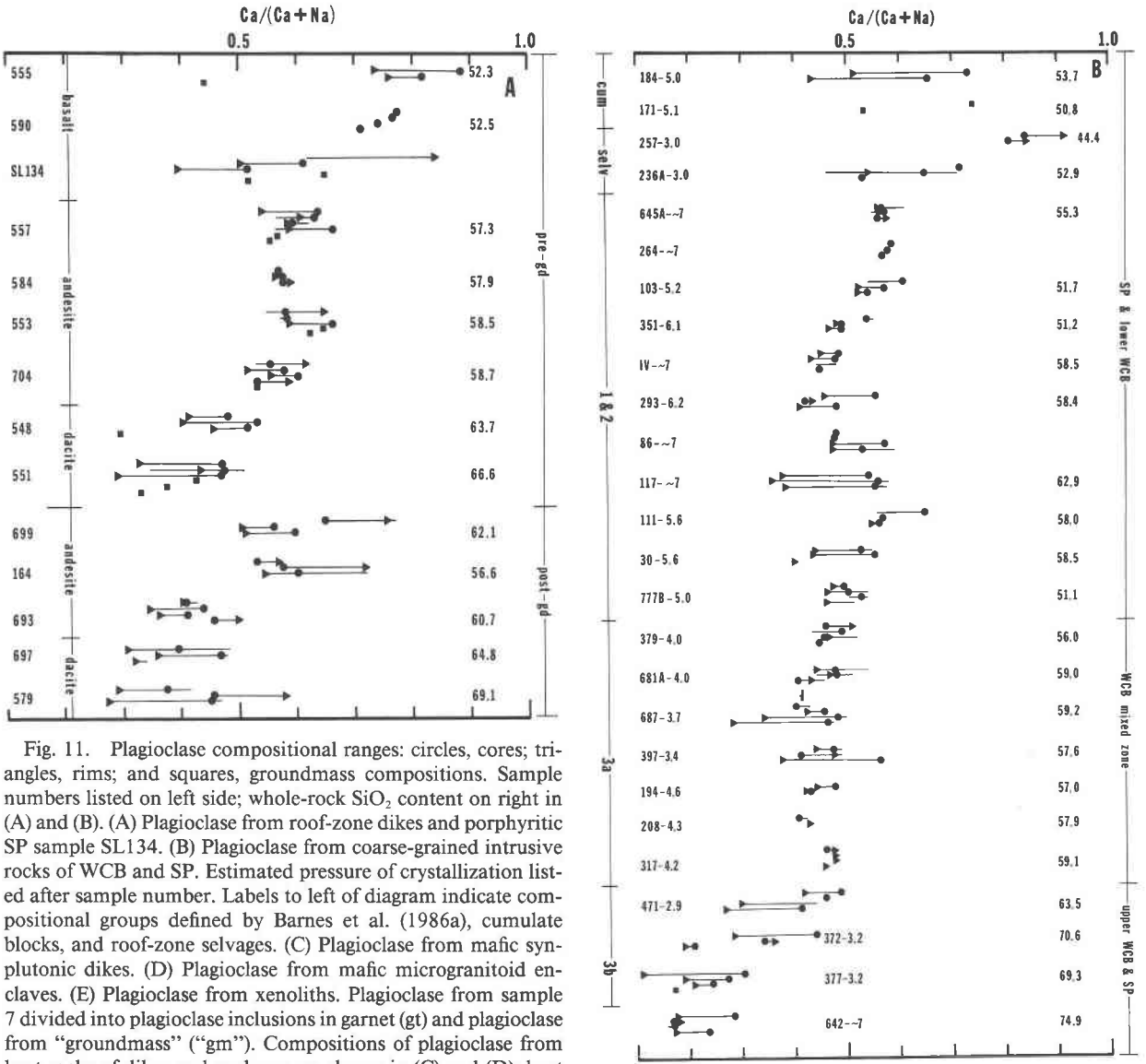

Fig. 11. Plagioclase compositional ranges: circles, cores; triangles, rims; and squares, groundmass compositions. Sample numbers listed on left side; whole-rock SiO_2 content on right in (A) and (B). (A) Plagioclase from roof-zone dikes and porphyritic SP sample SL134. (B) Plagioclase from coarse-grained intrusive rocks of WCB and SP. Estimated pressure of crystallization listed after sample number. Labels to left of diagram indicate compositional groups defined by Barnes et al. (1986a), cumulate blocks, and roof-zone selvages. (C) Plagioclase from mafic synplutonic dikes. (D) Plagioclase from mafic microgranitoid enclaves. (E) Plagioclase from xenoliths. Plagioclase from sample 7 divided into plagioclase inclusions in garnet (gt) and plagioclase from "groundmass" ("gm"). Compositions of plagioclase from host rocks of dikes and enclaves are shown in (C) and (D); host sample numbers are enclosed in brackets.

pyroxene and very coarse-grained amphibole (App. 1). Late-stage growth of calcic amphibole in this sample may have resulted in relatively Na-rich plagioclase.

Figure 11D shows plagioclase compositions for host–mafic microgranitoid enclave pairs. As was true with hornblende compositions, enclave 681 has plagioclase compositions very similar to the host, but enclaves 686B and 686E have plagioclase that is more calcic than host-rock plagioclase. Note the compositional reversals in all of the enclave plagioclase.

Plagioclase compositions from xenoliths are shown in Figure 11E. Most show weak zoning in the range An_{57} to An_{43}, but plagioclase in xenolith 219A has calcic cores and that in xenolith 214B is unzoned bytownite. Sample 7B is a garnet + hornblende metagabbro (App. 1). Plagioclase inclusions in garnet are An rich, whereas both An-rich and intermediate plagioclase occur in the matrix (Fig. 11E). Both types of matrix plagioclase appear to be zoned toward ~An_{58} rims, a composition similar to the most calcic plagioclase in nearby host rocks of the Wooley Creek batholith. The calcic cores of the matrix plagioclase crystals are highy resorbed and appear to represent primary igneous compositions that were locally preserved by inclusion in garnet poikiloblasts.

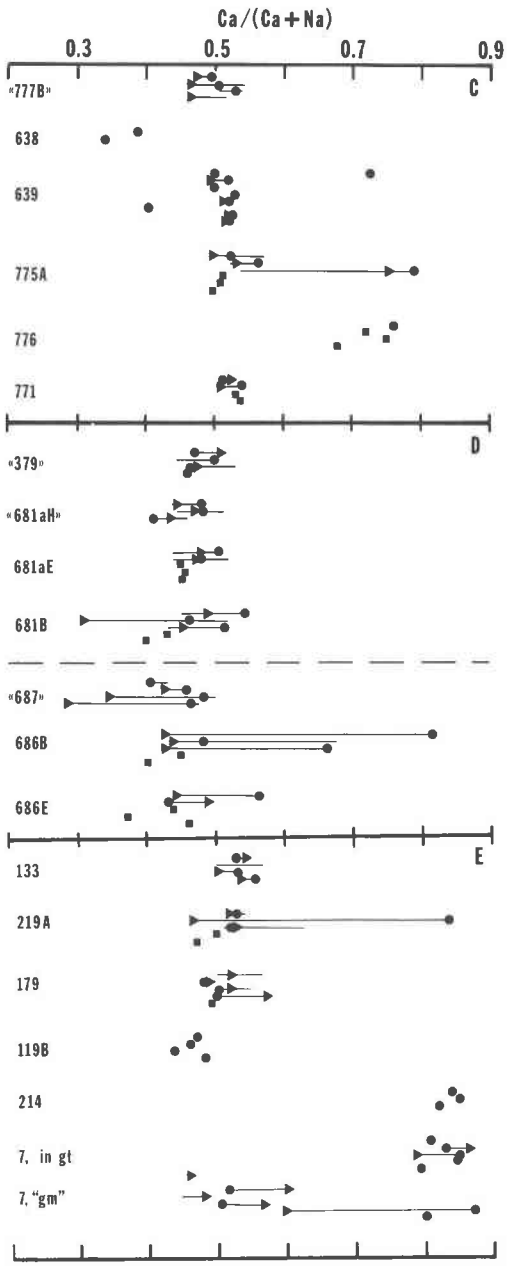

Fig. 11.—*Continued.*

Origin of zoning. Barnes et al. (1986a) used the composition of plagioclase phenocrysts in roof-zone dikes to try to relate the dikes to a corresponding structural level of the subjacent pluton in which similar plagioclase occurred. The assumption necessary for such a correlation is that slow cooling of the plutonic rocks did not result in appreciable adjustment of plagioclase (especially core) compositions. Data for the mafic synplutonic dikes and metasedimentary mafic enclaves (Figs. 11C, 11D) indicate a tendency for plagioclase compositions to approach those of the host, in spite of the difference in bulk compositions. Nevertheless, core compositions indicate that equilibration with the host was at least locally incomplete. Thus, if slow cooling did not completely modify plagioclase in these mafic rocks, it seems likely that the core compositions of plagioclase in the host pluton reflect primary magmatic conditions.

If the assumption above is correct, then the following correlations can be made. Mafic selvages of the Wooley Creek batholith roof zone, cumulate gabbroic blocks in the Wooley Creek batholith, metagabbro xenolith 7B, and some of the mafic synplutonic dikes have plagioclase core compositions similar to plagioclase in the basaltic roof-zone dikes. Barnes et al. (1986a) interpreted the various rocks listed above to have accumulated from early basaltic liquid in the WCB-SP system. In view of the plagioclase composition from some of the mafic synplutonic dikes, it is also possible that some "cumulate" blocks formed from slowly cooled mafic magma that was injected into the system and later disrupted by convection. Group 1 plutonic rocks have plagioclase core compositions that overlap those of the roof-zone andesitic and dacitic dikes, with the majority most similar to plagioclase in the andesites. Group 1 rocks with predominantly andesine cores (IV, 293, 351) are strongly foliated (protoclastic to cataclastic) and typically show complete reaction of pyroxene to hornblende. This reaction probably resulted in an increase in the Ab content of the coexisting plagioclase. Therefore, it seems likely that all of the group 1 rocks originally contained labradoritic plagioclase similar to the roof-zone andesite. Group 2 and 3 rocks have plagioclase core compositions similar to plagioclase in roof-zone dacitic dikes. It is interesting to note that the group 2 and 3 samples have estimated crystallization pressures of less than 5 kbar, whereas, with the exception of mafic roof-zone selvages, group 1 samples have estimated pressures greater than or equal to 5 kbar. Also note that among the plutonic plagioclase, only roof-zone selvage 257A and group 2 samples have significant reverse zoning (Figure 11B). These zoning patterns may reflect the location of the samples within the system: the roof-zone for gabbro selvage 257A, and the zone rich in mafic microgranitoid enclaves for group 2.

Possible origins for reverse zoning in plagioclase include slow diffusion of constituent cations (at least for thin oscillations, Bottinga et al., 1966), isothermal decrease in total pressure, increase in the partial pressure of H_2O (Loomis, 1982), and influx and mingling of new magma with higher Ca content than the original magma (e.g., Sakuyama, 1981; Hibbard, 1981). Of these processes, the most effective ones appear to be increase in partial pressure of H_2O (Loomis, 1982) and magma mixing. Barnes (1983) suggested that both processes occurred in the Wooley Creek batholith, and Barnes et al. (1986a) extended those conclusions to the entire system. Major- and trace-element data show that group 3 rocks are distinct from group 1 rocks because of an early upward enrichment of H_2O in the magmatic system (Barnes, 1983). Under such conditions, early roof-zone cumulates such as 257A would be expected to show reversely zoned pla-

TABLE 8. Representative alkali feldspar analyses

	317-1	317-2	377-1	377-2	579-1	579-3	642A-1
			Compositions in wt%				
SiO_2	63.01	64.83	65.10	64.18	64.24	65.07	63.71
Al_2O_3	18.82	18.48	18.30	18.77	18.74	18.41	18.77
FeO	0.36	0.09	0.09	0.09	0.01	0.03	0.01
CaO	0.00	0.00	0.03	0.07	0.08	0.01	0.03
Na_2O	1.21	0.80	1.52	2.57	2.13	1.38	1.13
K_2O	14.11	15.64	14.50	12.21	12.58	14.37	14.20
BaO	1.72	0.13	0.16	1.89	2.23	0.09	1.71
ZnO	0.00	0.06	0.04	0.03	0.00	0.04	0.02
Total	99.23	100.03	99.75	99.82	100.01	99.40	99.59
			Cations per eight oxygens				
Si	2.957	2.993	3.001	2.972	2.977	3.003	2.971
Al	1.041	1.005	0.994	1.024	1.022	1.001	1.032
Fe	0.014	0.002	0.002	0.002	0.000	0.000	0.000
Ca	0.000	0.000	0.001	0.002	0.002	0.000	0.001
Na	0.110	0.070	0.135	0.231	0.190	0.123	0.101
K	0.845	0.921	0.852	0.720	0.742	0.845	0.844
Ba	0.032	0.001	0.002	0.034	0.039	0.001	0.030
Zn	0.000	0.001	0.000	0.000	0.000	0.000	0.000
Total	5.000	4.993	4.987	4.986	4.973	4.973	4.979

gioclase, as is the case. Reverse zoning in group 2 plagioclase is probably the result of magma mixing, either of newly injected basaltic magma with the host (Barnes, 1983), or of group 1 with group 3 magmas in an interface zone separating the two (Barnes et al., 1986a). At this writing, the second hypothesis is preferred, for reasons given by Barnes et al. (1986a).

Reversed zoning of plagioclase in roof-zone andesite is best explained by a magma-mixing process in which injected basaltic magma mixed with mostly liquid magma in the lower part of the chamber. Such a process would explain the wider excursions in reversed zoning among the roof-zone andesite dikes and the paucity of crystal clots or enclaves in these dikes. Speculation as to the reasons for the two types of zoning will be presented in a later section.

Alkali feldspar

Alkali feldspar in the WCB-SP occurs as poikilitic to interstitial crystals (typically microcline), with oikocrysts as much as 2 cm in diameter. In the roof-zone dacitic dikes, interstitial microcline and granophyric intergrowths are the common forms of alkali feldspar. Microprobe analyses show that the alkali feldspar contains negligible Ca, Fe, and Sr. The analyses also show a bimodal distribution of alkali feldspar compositions (Table 8). One group of analyses are of nearly pure microcline with less than 0.2 wt% BaO; the second group ranges from Or_{92} to Or_{75} and contains 0.8 to 2.3 wt% BaO. The two compositions occur not only in the same sample but, in some cases, in the same grain. Compositionally distinct parts of alkali feldspar crystals appear to be randomly distributed and are not separated by an optical discontinuity. Similar intracrystalline variation was observed in alkali feldspar from a group of Sierran granitoids by Piwinskii (1968).

In spite of the large variations in alkali feldspar composition, an attempt was made to apply the two-feldspar geothermometer of Stormer (1975) to these samples. Temperature estimates used an average composition of Ba-rich alkali feldspar and the rim composition of coexisting plagioclase. The results for all of the two-feldspar pairs yielded temperature estimates of less than 600°C.

Estimates of intensive variables

One of the goals of this study was to attempt estimates of temperature, f_{O_2}, and f_{H_2O} in the WCB-SP system by using mineral assemblages and compositions in the roof-zone dikes. In some cases, moderate success was achieved, but in others, only crude estimates can be made. Inasmuch as the estimates discussed below depend on paragenetic relations among the roof-zone dikes, a brief review of the order of phenocryst stability follows (after Barnes, 1983; Barnes et al., 1986a). In basaltic and basaltic andesite dikes, clinopyroxene + magnetite (± olivine) were the first phases to crystallize, followed by ilmenite, plagioclase, and rare orthopyroxene. In the early andesitic dikes, clinopyroxene + magnetite were followed by plagioclase + orthopyroxene + ilmenite, then by hornblende as thin rims on pyroxene. Early and late dacitic dikes show relict orthopyroxene, then hornblende + plagioclase ± ilmenite, followed by quartz and biotite (both as phenocrysts). Alkali feldspar occurs only as a groundmass phase. Late andesitic dikes show both the two-pyroxene paragenesis listed above and a clinopyroxene + plagioclase + hornblende paragenesis displayed by sample 693 (App. 1).

Temperature

Application of pyroxene geothermometry on clinopyroxene (see above) yields temperature estimates for pyroxene-bearing roof-zone dike samples in the range of 960 to 1120°C. The stability of hornblende in roof-zone andesite allows comparison with numerous experimental

studies on similar compositions (e.g., Eggler, 1972; Eggler and Burnham, 1973; Ritchey and Eggler, 1978). These studies show that at moderate H_2O concentrations, hornblende is stable at temperatures in the range 940 to 975°C. An estimated pyroxene temperature from hornblende + pyroxene andesite sample 693 yields 963°C, in accord with the experimental studies. The variation in minor-element concentrations in individual hornblende crystals also suggests that hornblende crystallized over a relatively large temperature range.

Oxygen fugacity

The fugacity of oxygen can be estimated for the two-pyroxene andesite and basaltic andesite compositions (see above) to lie slightly above NNO (Fig. 10). Wones (1981) and Noyes et al. (1983) used the equilibrium

$$\underset{\text{titanite}}{3CaTiSiO_5} + \underset{\text{magnetite}}{2Fe_3O_4} + \underset{\text{quartz}}{3SiO_2} = \underset{\text{hedenbergite}}{3CaFeSi_2O_6} + \underset{\text{ilmenite}}{3FeTiO_3} + O_2$$

as a limiting assemblage for f_{O_2} conditions in rocks that contain titanite, clinopyroxene, magnetite, ilmenite, and quartz (TMQH). Noyes et al. (1983) also suggested that a similar equilibrium could be written with amphibole replacing clinopyroxene ("TMQA buffer"). These two equilibrium boundaries are plotted in Figure 10 and both lie at f_{O_2} conditions higher than those estimated for the roof-zone dikes. The positions of these equilibria are in accord with the absence of primary titanite in all WCB-SP rocks except those from the late stock in the southern Wooley Creek batholith (sample 377, Fig. 2). If one assumes that the late stock is a differentiation product of the WCB-SP system, then two temperature-f_{O_2} paths can be used to constrain fugacity conditions in the system. The first path is shown as a stippled band on Figure 10. It is subparallel to, and at slightly higher f_{O_2} than, NNO until low temperature conditions are reached. With further cooling, f_{O_2} remains approximately constant, intersects the TMQA equilibrium (sample 377), then continues in subsolidus conditions to the HM buffer, where magnetite is oxidized to hematite in slowly cooled samples (see above). The second path (not shown) crosses the TMQH equilibrium and approaches TMQA conditions at higher temperatures than the first. Either path is in accord with Fe^{+3}/Fe^{+2} in biotites from samples 471 and 377 (Table 5) that indicates f_{O_2} between NNO and HM (Fig. 8).

Water content

Determination of f_{O_2} or X_{H_2O} in magmas has typically proved to be difficult for granitoid rocks. This project is no exception. In general, X_{H_2O} can be estimated by comparison of observed paragenetic sequences with experimental studies of similar bulk compositions under similar f_{O_2}-pressure-temperature conditions. Few such studies are available for compositions like those of the WCB-SP system. For example, most experiments on basaltic compositions have been carried out either under anhydrous conditions or at $P_{H_2O} = P_{total}$, whereas experiments on andesitic compositions have been carried out on samples considerably more aluminous than those dealt with here. Because of these factors, the following conclusions are, at best, rough estimates.

In basaltic compositions, early stability of augite (with olivine absent or rare) suggests relatively H_2O-rich conditions at moderate P_{total}. At low P_{total} or P_{H_2O}, either olivine or plagioclase is the liquidus phase, depending on bulk composition (e.g., Yoder and Tilley, 1962; Grove et al., 1982; Grove and Bryan, 1983). In 1-atm experiments on high-alumina basalts and basaltic andesite, Grove et al. (1982) found pigeonite to be the high-temperature low-Ca pyroxene. Allen and Boettcher (1978) found clinopyroxene to be the liquidus phase in olivine tholeiite at 10-kbar pressure and for a range of X_{H_2O} (on the HM buffer). Several of the basaltic roof-zone dikes contain interstitial magmatic hornblende rimming or replacing clinopyroxene, and hornblende phenocrysts are common among mafic synplutonic dikes. Although experimental studies of H_2O-undersaturated basaltic magmas at moderate P_{total} (3 to 7 kbar) are rare or lacking, comparison with hornblende stability fields in andesites suggests that H_2O in the range 2 to 4 wt% is necessary in order to stabilize hornblende above the solidus.

Similarly, the liquidus phase of andesitic magmas at low P_{total} is plagioclase (Eggler, 1972; Eggler and Burnham, 1973; Grove et al., 1982). However, at higher pressure and under H_2O-undersaturated conditions, pyroxene replaces plagioclase as the liquidus phase. At a pressure appropriate for the WCB-SP (5 kbar), the experiments indicate that hornblende is not a stable phase unless the H_2O concentration in the *melt* is greater than about 4 wt% (Eggler and Burnham, 1973).

Dacitic dikes contain relict orthopyroxene, with plagioclase, hornblende, biotite, and quartz phenocrysts. The experiments of Piwinskii (1973) on granodioritic compositions at $P_{H_2O} = P_{total}$ indicate that quartz is a near-solidus phase. Studies of synthetic granodiorite and granite (Naney, 1983; Whitney, 1975) show that the stability field of quartz expands relative to alkali feldspar if $P_{H_2O} < P_{total}$. Naney's (1983) results for synthetic granodiorite with H_2O contents between about 3.8 and 4.8 wt% reproduce the order of crystallization of the roof-zone dactite: plagioclase, orthopyroxene, hornblende, biotite, and finally quartz. These values correspond to somewhat higher concentrations of H_2O in the *melt,* depending on the crystallinity of the magma.

It is interesting to note that some of the quartz dioritic and gabbroic samples of the Wooley Creek batholith lack hornblende and contain the mafic assemblage clinopyroxene + orthopyroxene + biotite ± oxides. Naney's (1983) work on more felsic compositions suggests that the pyroxene + biotite assemblage is indicative of relatively low P_{H_2O}. The distribution of such samples is scat-

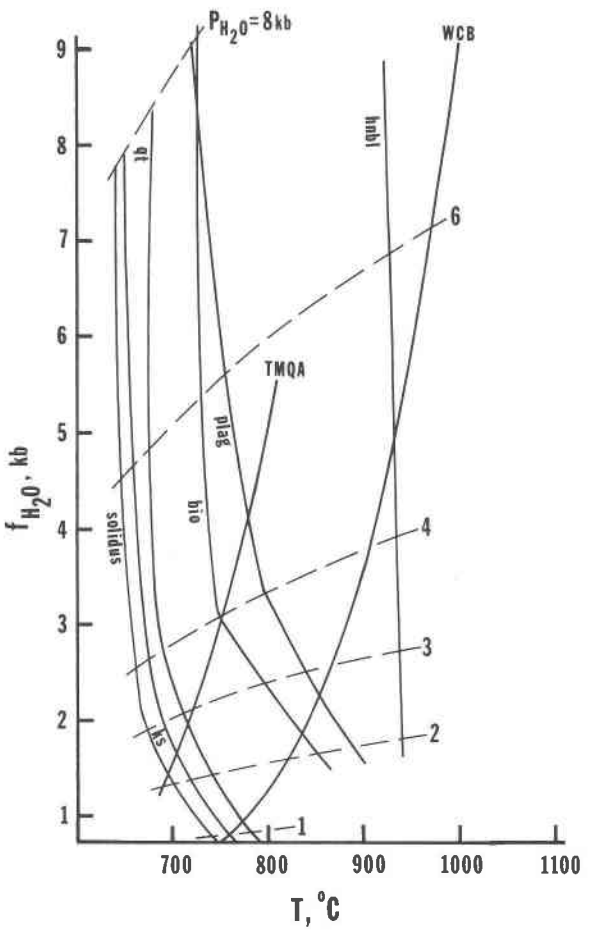

Fig. 12. H_2O-saturated phase relations for the Mt. Givens granodiorite (Piwinskii, 1973) plotted as a function of the fugacity of H_2O. Curves labeled TMQA and WCB are for the equilibrium among K-feldspar, magnetite, biotite, and quartz in which f_{O_2} is defined by the TMQA buffer and the estimate of f_{O_2} for the WCB (Fig. 10), respectively. Dashed curves are isobars. See text for discussion.

tered but restricted to parts of the system in which P_{total} is estimated to be >4.5 kbar. If these amphibole-free rocks crystallized under H_2O-poor conditions, it appears that at least the deep parts of the WCB-SP system were heterogeneous with regard to H_2O content.

Fugacity of H_2O in roof-zone granodiorite sample 471 was estimated using the equilibrium

$$\underset{\text{annite}}{KFe_3^{2+}AlSi_3O_{10}(OH)_2} + \tfrac{1}{2}O_2 = \underset{\substack{\text{alkali}\\ \text{feldspar}}}{KAlSi_3O_8} + \underset{\text{magnetite}}{Fe_3O_4} + H_2O.$$

Wones (1972) expressed the equilibrium constant as $\log_{10}K_{annite} = 7409/T + 4.25$, where T is in kelvins and

$$K_{annite} = \frac{a_{Or}^{Ksp}\, a_{Fe_3O_4}^{Mt}\, f_{H_2O}}{a_{Ann}^{Bio}\, f_{O_2}^{1/2}}$$

and a_i = activity of component i and f_j = fugacity of component j, Or = $KAlSi_3O_8$, Ann = $KFe_3AlSi_3O_{10}(OH)_2$, Mt = magnetite, Bio = biotite, and Ksp = alkali feldspar. For this estimate, activity-composition relationships are assumed to be $a_{Fe_3O_4}^{Mt} = 1$, $a_{Or}^{Ksp} = X_{Or}^{Ksp} = 0.75$, $a_{Ann}^{Bio} = (X_{Fe}^{oct})^3$, and f_{O_2} defined by the temperature-f_{O_2} path shown in Figure 10 and TMQA [see Noyes et al. (1983) for a similar procedure]. The assumption of ideality in biotite cannot be correct for a sample so rich in Fe^{3+}, but appropriate activity-composition relations are unknown. Figure 12 shows the estimated equilibrium boundaries in temperature-f_{H_2O} space. The H_2O-saturated phase boundaries for Mt. Givens granodiorite (Piwinskii, 1973) are also shown in Figure 12, as are 1-, 2-, 3-, 4-, and 6-kbar isobars. The intersection of the biotite stability estimates with the solidus should provide an estimate of maximum f_{H_2O} and, by interpolation, P_{H_2O} at near-solidus conditions. The curve based on the f_{O_2} path from Figure 10 gives $P_{H_2O} < 1$ kbar, whereas the curve based on TMQA gives P_{H_2O} slightly greater than 2 kbar. The latter estimate is in rough agreement with estimates of P_{total} and the H_2O-rich, but undersaturated, nature of the felsic Wooley Creek batholith magma. The reader should take into account the numerous uncertainties and approximations before giving much credence to this approach.

Discussion

Dikes in the roof-zone of the WCB-SP show strong mineralogical and bulk compositional similarities to the subjacent plutonic rocks. Therefore, dike compositions and phenocryst assemblages can be used to correlate the dikes with their coarse-grained cumulate counterparts. Correlations can be made on the basis of the following evidence: (1) two-pyroxene assemblages with labradoritic plagioclase are predominant in the lower parts of each pluton, especially "below" the 4.5- to 5.0-kbar level (Fig. 2) and in roof-zone andesite, (2) hornblende is a near-liquidus phase only in plutonic samples "above" the 4.5-kbar level (Barnes, 1983) and in roof-zone dacite, (3) anorthitic plagioclase similar to that in roof-zone basaltic dikes is present in the plutonic rocks, but only in selvages, cumulate blocks, mafic microgranitoid enclaves (rarely), and mafic synplutonic dikes.

Thus, one can conclude that the roof-zone dikes correlate with the plutonic constituents as follows: Roof-zone basalt dikes are cogenetic with the synplutonic dikes and the mafic microgranitoid enclaves and represent the initial magma pulses in the chamber. Roof-zone andesite dikes were derived from magma that crystallized to form gabbro to mafic tonalite in the lower part of the system, and roof-zone dacite dikes were derived from magma that crystallized to form tonalite to granite in the upper part of the system. Average plagioclase compositions (Figs. 11A and 11B) support this correlation, but discrepancies in zoning patterns between plutonic and roof-zone plagioclase suggest a more complicated story, as discussed below.

Barnes (1983) interpreted the gradational-upward zon-

ing in the system to be the result of crystal accumulation from a basaltic parent with accompanying upward boundary-layer flow of fractionated liquid to form a lighter, H_2O-rich, felsic cap (McBirney, 1980; Nilson et al., 1985). The correlations made above suggest a simpler stratigraphy in which mafic andesite was overlain by dacite. The gradational-upward zonation reported by Barnes (1983) is probably due to more efficient crystal accumulation in deeper levels of the system.

One of the interesting results of this study is the recognition of relativley minor zoning in both pyroxene and plagioclase of the roof-zone andesite and "correlative" two-pyroxene plutonic rocks. Furthermore, plagioclase with reverse zoning is common in the roof-zone andesite, but rare in the corresponding plutonic rocks (Figs. 11A and 11B). These differences can be explained if the lower part of the chamber was filled with a hot, actively convecting andesitic melt that received periodic basaltic replenishment from below. As the lower part of the pluton cooled, pyroxene and plagioclase nucleated and grew on the chamber walls. Fractionated liquid resulting from this crystal growth was richer in SiO_2 and H_2O and less dense than the adjacent magma (e.g., McBirney, 1980; Spera et al., 1982; Nilson et al., 1985) and rose by boundary-layer flow. Some fractionated liquid was mixed back into the convecting interior, some underwent further fractionation due to side-wall crystallization, and the rest rose to the roof-zone where it accumulated to form the dacitic cap. Influxes of basaltic magma presumably rose through the base of the system along a preheated conduit (e.g., Hildreth, 1981; Marsh, 1982) and had little contact with the crystal mush at the walls. Because of the volume of the chamber (minimum of 750 km^3; Barnes, 1982), each basaltic influx probably could not affect the entire chamber or cause chamber-wide convective overturn (e.g., Huppert and Sparks, 1980) but instead initially mingled with a smaller magma volume. Such mingling would be expected to produce local reversed zoning in plagioclase, clinopyroxene rims on orthopyroxene (e.g., Sakuyama, 1981, 1984; Gerlach and Grove, 1982), and elevated abundances of Rb and Zr, all of which are seen in roof-zone andesite (Barnes et al., 1986a).

If the influx of basaltic magma was initially sufficient to offset the effects of crystal fractionation along the chamber's margins, then the time-averaged composition of the lower part of the chamber would have remained relatively constant. Thus, the rocks that crystallized along the chamber walls would have formed from a relatively uniform composition and would have been weakly zoned. The lower part of the pluton can be regarded as having been buffered by the magma-mixing process.

The dacitic cap grew downward and stoped upward (Barnes, 1983) until fractionated magma from below was no longer available. Evidence for substantial magma mixing in the magma that formed the early (i.e., prior to crystallization of Wooley Creek batholith granodiorite) dacitic dikes is weak or absent. Plagioclase is predominantly normally zoned, and hornblende shows no sharp changes in Mg/(Mg + Fe). The same holds true for the correlative tonalitic to granitic rocks of the pluton.

In contrast, late-stage dacites and hornblende + pyroxene andesites in the roof zone contain reversely zoned plagioclase, and the andesites commonly contain xenocrysts of quartz with amphibole coronas (Barnes et al., 1986a). These features were interpreted by Barnes et al. (1986a) to result from magma mixing in the interior of a largely crystalline magmatic system. The remaining magma, because of its relatively small volume, would no longer have been able to buffer influxes of basaltic magma. As a result, the correlative plutonic rocks should show evidence of reversely zoned plagioclase. The best candidates for such rocks are samples 379 and 397 (Fig. 11B), which were collected within the upper part of the enclave-rich zone of the WCB (Fig. 2).

Late-stage magmas apparently crystallized under relatively more oxidizing conditions. This is shown by the presence of primary titanite and Mg-rich biotite and hornblende in late-stage granite (sample 377) and may explain the Mg-rich clinopyroxene in late-stage roof-zone andesite (sample 693, Table 3).

Conclusions

The WCB and SP represent a vertically extensive magmatic system that was periodically tapped to form roof-zone dikes. Mineral compositions and zoning, paragenetic relations, and temporal relations among the roof-zone dikes indicate that (1) the WCB-SP evolved from a predominantly andesitic system to one with andesite overlain by a dacitic cap; (2) through most of its history, f_{O_2} values in the system were slightly higher than NNO; (3) f_{O_2} probably was not buffered at low T, resulting in Mg-rich mafic minerals and primary titanite in late granitic liquids and hematite in subsolidus conditions; (4) the magma was H_2O-rich but probably undersaturated until near-solidus conditions were reached; (5) P effects on mineral compositions were minor and apparently restricted to greater Al content in clinopyroxene and hornblende at higher pressure. The relative lack of upward compositional zoning among WCB-SP minerals can be explained as the result of the simple magmatic stratigraphy and of buffering of magma compositions by magma mixing in the lower part of the system.

Acknowledgments

C. M. Allen kindly provided samples of the Slinkard pluton and insight into their geologic setting. I am indebted to J. Hammarstrom and E-an Zen for their interest in this project and for numerous hornblende analyses. Reviews by G. K. Czamanske and an anonymous reviewer are greatly appreciated. Thanks are also due to D. Deuring for assistance with microprobe analyses and to M. Barnes for help in the field and laboratory. This work was supported by NSF Grant EAR-8408319.

References cited

Allen, C.M. (1982) Intrusive relations and petrography of the Slinkard pluton, central Kalmath Mountains, California. M.S. thesis, University of Oregon, Eugene, 120 p.

Allen, J.C., and Boettcher, A.L. (1978) Amphiboles in andesite and basalt:

II. Stability as a function of P-T-f_{H_2O}-f_{O_2}. American Mineralogist, 63, 1074–1087.

Barnes, C.G. (1982) Geology and petrology of the Wooley Creek batholith, Klamath Mountains, northern California. Ph.D. thesis, University of Oregon, Eugene.

——— (1983) Petrology and upward zonation of the Wooley Creek batholith, Klamath Mountains, California. Journal of Petrology, 24, 495–537.

Barnes, C.G., Allen, C.M., and Saleeby, J.B. (1986a) Open- and closed-system characteristics of a tilted plutonic system, Klamath Mountains, California. Journal of Geophysical Research, 91, 6073–6090.

Barnes, C.G., Rice, J.M., and Gribble, R.F. (1986b) Tilted plutons in the Klamath Mountains of California and Oregon. Journal of Geophysical Research, 91, 6059–6071.

Bateman, P.C., and Chappell, B.W. (1979) Crystallization, fractionation, and solidification of the Tuolumne Intrusive Series, Yosemite National Park, California. Geological Society of America Bulletin, 90, Part I, 465–482.

Bateman, P.C., and Eaton, J.P. (1967) Sierra Nevada batholith. Science, 158, 1407–1417.

Bickner, F.R. (1977) A general petrologic study of the Bear Creek metagabbros, their almandine garnet and associated rocks within the Wooley Creek batholith. Senior thesis, Humboldt State University, Arcata, 69 p.

Blake, M.C., Jr., Howell, D.G., and Jones, D.L. (1982) Preliminary tectonostratigraphic terrane map of California. U.S. Geological Survey Open-File Report 82-593.

Bottinga, Y., Kuda, A., and Weill, D. (1966) Some observations on oscillatory zoning and crystallization of magmatic plagioclase. American Mineralogist, 51, 792–806.

Bussell, M.A. (1985) The centered complex of the Rio Huaura: A study of magma mixing and differentiation in high-level magma chambers. In W.S. Pitcher, et al., Eds., Magmatism at a plate edge: The Peruvian Andes, p. 128–155. Halsted Press, New York.

Cater, F.W. (1982) Intrusive rocks of the Holden and Lucerne quadrangles, Washington—The relation of depth zones, composition, textures, and emplacement of plutons. U.S. Geological Survey Professional Paper 1220, 108 p.

Chou, I-M. (1978) Calibration of oxygen buffers at elevated pressure and temperature using the hydrogen fugacity sensor. American Mineralogist, 63, 690–703.

Christiansen, R.L., Lipman, P.W., Carr, W.J., Byers, F.M., Jr., Orkild, P.P., and Sargent, K.A. (1977) Timber Mountain–Oasis Valley caldera complex of southern Nevada. Geological Society of America Bulletin, 88, 943–959.

Coleman, R.G., Mortimer, N., Donato, M.M., Manning, C.E., and Hill, L.B. (1987) Tectonic and regional metamorphic framework of the Klamath Mountains and adjacent Coast Ranges, California and Oregon. In W.G. Ernst, Ed., Rubey Volume 7. Prentice-Hall, Englewood Cliffs, New Jersey, in press.

Czamanske, G.K., Ishihara, S., and Atkin, S.A. (1981) Chemistry of rock-forming minerals of the Cretaceous-Paleocene batholith in southwestern Japan and implications for magma genesis. Journal of Geophysical Research, 86, 10431–10469.

Dellinger, D.A., and Hopson, C.A. (1986) Age-depth compositional spectrum through the diapiric Duncan Hill pluton, North Cascades, Washington. Geological Society of America Abstracts with Programs, 18, 100–101.

Didier, J. (1973) Granites and their enclaves: The bearing of enclaves on the origin of granites. Elsevier, New York, 393 p.

Dodge, F.C.W., Smith, V.C., and Mays, R.E. (1969) Biotites from granitic rocks of the central Sierra Nevada batholith, California. Journal of Petrology, 10, 250–271.

Eggler, D.H. (1972) Water-saturated and undersaturated melting relations in a Paricutin andesite and an estimate of water content in the natural magma. Contributions to Mineralogy and Petrology, 34, 261–271.

Eggler, D.H., and Burnham, C.W. (1973) Crystallization and fractionation trends in the system andesite-H_2O-CO_2-O_2 at pressures to 10 kb. Geological Society of America Bulletin, 84, 2517–2532.

Flood, R.H., and Shaw, S.E. (1979) K-rich cumulate diorite at the base of a tilted granodiorite pluton from the New England batholith, Australia. Journal of Geology, 87, 417–425.

Furman, T.H., and Spera, F.J. (1984) Mafic inclusions in granitoid plutons: Basic melt intruded during crystallization. In M.A. Dungan, T.L. Grove, and W. Hildreth, Eds., Proceedings of the Conference on Open Magmatic Systems, ISEM, SMU, Dallas, 49–51.

Gerlach, D.C., and Grove, T.L. (1982) Petrology of Medicine Lake Highland volcanics: Characterization of end members of magma mixing. Contributions to Mineralogy and Petrology, 80, 147–159.

Gill, J.B. (1981) Orogenic andesites and plate tectonics. Springer-Verlag, New York, 390 p.

Grove, T.L., and Bryan, W.B. (1983) Fractionation of pyroxene-phyric MORB at low pressure: An experimental study. Contributions to Mineralogy and Petrology, 84, 293–309.

Grove, T.L., Gerlach, D.C., and Sando, T.W. (1982) Origin of calc-alkaline series lavas at Medicine Lake volcano by fractionation, assimilation and mixing. Contributions to Mineralogy and Petrology, 80, 160–182.

Grover, T.W. (1984) Progressive metamorphism west of the Condrey Mountain dome, north-central Klamath Mountains, northern California. M.S. thesis, University of Oregon, Eugene, 129 p.

Haggerty, S.E. (1976a) Oxidation of opaque mineral oxides in basalts. Mineralogical Society of America Reviews in Mineralogy, 3, Hg-1–Hg-100.

——— (1976b) Opaque mineral oxides in terrestrial igneous rocks. Mineralogical Society of America Reviews in Mineralogy, 3, Hg-101–Hg-276.

Hammarstrom, J. (1984) Microprobe analyses of hornblendes from 5 calc-alkalic intrusive complexes with data tables for other calcic amphiboles and BASIC computer programs for data manipulation. U.S. Geological Society Open-File Report 84-652, 98 p.

Hammarstrom, J.M., and Zen, E-an. (1986) Aluminum in hornblende: An empirical igneous geobarometer. American Mineralogist, 71, 1297–1313.

Harper, G.D., and Wright, J.E. (1984) Middle to Late Jurassic tectonic evolution of the Klamath Mountains, California-Oregon. Tectonics, 3, 759–772.

Hawthorne, F.C. (1981) Crystal chemistry of the amphiboles. Mineralogical Society of America Reviews in Mineralogy, 9A, 1–102.

Hewitt, D.A. (1978) A redetermination of the fayalite-magnetite-quartz equilibrium between 650° and 850°. American Journal of Science, 278, 715–724.

Hibbard, M.J. (1981) The magma mixing origin of mantled feldspars. Contributions to Mineralogy and Petrology, 76, 158–170.

Hildreth, W. (1981) Gradients in silicic magma chambers: Implications for lithospheric magmatism. Journal of Geophysical Research, 86, 10153–10192.

Huppert, H.E., and Sparks, R.S.J. (1980) The fluid dynamics of a basaltic magma chamber replenished by influx of hot, dense ultrabasic magma. Contributions to Mineralogy and Petrology, 75, 279–289.

Irwin, W.P. (1960) Geologic reconnaissance of the northern Coast Ranges and Klamath Mountains, with a summary of the mineral resources. California Division of Mines and Geology Bulletin, 179, 1–80.

——— (1966) Geology of the Klamath Mountains province. Geology of Northern California. California Division of Mines and Geology Bulletin, 190, 19–38.

——— (1972) Terrains of the western Paleozoic and Triassic belt in the southern Klamath Mountains, California. U.S. Geological Survey Professional Paper 800-C, C103–C111.

——— (1981) Tectonic accretion of the Klamath Mountains. In W.G. Ernst, Ed., The geotectonic development of California, p. 29–49. Prentice-Hall, Englewood Cliffs, N.J.

——— (1985) Age and tectonics of plutonic belts in accreted terranes of the Klamath Mountains, California and Oregon. In D.G. Howell, Ed., Tectonostratigraphic terranes of the circum-Pacific region. Circum-Pacific Council for Energy and Mineral Resources, Earth Science Series, 1, 187–199.

Jachens, R.C., Barnes, C.G., and Donato, M.M. (1986) Subsurface configuration of the Orleans fault: Implications for deformation in the western Klamath Mountains, California. Geological Society of America Bulletin, 97, 388–395.

Kretz, R. (1961) Some applications of theromdynamics to coexisting minerals of variable composition. Examples: Orthopyroxene-clinopyroxene and orthopyroxene-garnet. Journal of Geology, 69, 361–387.

——— (1982) Transfer and exchange equilibria in a portion of the pyroxene quadrilateral as deduced from natural and experimental data. Geochemica et Cosmochimica Acta, 46, 411–421.

Lieberman, J.E. (1983) Petrology and petrogenesis of marble and peridotite, Seiad ultramafic complex, California. M.S. thesis, University of Oregon, Eugene, 119 p.

Lindsley, D.H. (1983) Pyroxene thermometry. American Mineralogist, 68, 477–493.

Lindsley, D.H., and Andersen, D.J. (1983) A two-pyroxene thermometer. Proceedings of the the 13th Lunar Planetary Science Conference, Part 2, Journal of Geophysical Research Supplement 88, A887–A906.

Loomis, T.P. (1982) Numerical simulations of crystallization processes of plagioclase in complex melts: The origin of major and oscillatory zoning in plagioclase. Contributions to Mineralogy and Petrology, 81, 219–229.

Marsh, B.D. (1982) On the mechanics of igneous diapirism, stoping, and zone melting. American Journal of Science, 282, 808–855.

McBirney, A.R. (1980) Mixing and unmixing of magmas. Journal of Volcanology and Geothermal Research, 7, 357–371.

McCarthy, T.S., and Hasty, R.A. (1976) Trace element distribution patterns and their relationship to the crystallization of granitic melts. Geochimica et Cosmochimica Acta, 40, 1351–1358.

Miller, C.F., Stoddard, E.F., Bradfish, L.J., and Dollase, W.A. (1981) Composition of plutonic muscovite: Genetic implications. Canadian Mineralogist, 19, 25–34.

Mortimer, N. (1985) Structural and metamorphic aspects of middle Jurassic terrane juxtaposition, northeastern Klamath Mountains, California. In D.G. Howell, Ed., Tectonostratigraphic terranes of the Circum-Pacific region. Circum-Pacific Council for Energy; and Mineral Resources, Earth Science Series, 1, 201–214.

Mortimer, N., and Coleman, R.G. (1985) A Neogene structural dome in the Klamath Mountains, California and Oregon. Geology, 13, 253–256.

Naney, M.T. (1983) Phase equilibria of rock-forming silicates in granitic systems. American Journal of Science, 283, 993–1033.

Nilson, R. H., McBirney, A.R., and Baker, B.H. (1985) Liquid fractionation. Part II: Fluid dynamics and quantitative implications for magmatic systems. Journal of Volcanology and Geothermal Research, 24, 25–54.

Noyes, H.J., Wones, D.R., and Frey, F.A. (1983) A tale of two plutons: Petrographic and mineralogic constraints on the petrogenesis of the Red Lake and Eagle Peak plutons, central Sierra Nevada, California. Journal of Geology, 91, 353–379.

Pabst, A. (1928) Observations on inclusions in the granitic rocks of the Sierra Nevada. University of California Publications, Department of Geological Sciences Bulletin, 17, 325–386.

Piwinskii, A.J. (1968) Experimental studies of igenous rock series, central Sierra Nevada batholith, California. Journal of Geology, 76, 548–570.

——— (1973) Experimental studies of igneous rock series, central Sierra Nevada batholith, California: Part II. Neues Jahrbuch für Mineralogie Montashefte, 193–215.

Reid, J.B., and Hamilton, M.A. (1985) Hornblendes in Sierra Nevadan granitoids: Fingerprints of the mafic component in mixed plutonic rocks. EOS, 66, 1132.

Reid, J.B., Jr., Evans, O.C., and Fates, D.G. (1983) Magma mixing in granitic rocks of the central Sierra Nevada, California. Earth and Planetary Science Letters, 66, 243–261.

Ritchey, J.R., and Eggler, D.H. (1978) Amphibole stability in a differentiated calc-alkaline magma chamber: An experimental investigation. Carnegie Institution of Washington Year Book 77, 790–793.

Robinson, Peter, Ross, M., and Jaffe, H.W. (1971) Composition of the anthophyllite-gedrite series, comparisons of gedrite-hornblende, and the anthophyllite-gedrite solvus. American Mineralogist, 56, 1005–1041.

Robinson, Peter, Spear, F.S., Schumacher, J.C., Laird, J., Klein, C., Evans, B.W., and Doolan, B.L. (1982) Phase relations of metamorphic amphiboles: Natural occurrence and theory. Mineralogical Society of America Reviews in Mineralogy, 9B, 1–227.

Sakuyama, M. (1981) Petrological study of the Myoko and Kurohime volcanoes, Japan: Crystallization sequence and evidence for magma mixing. Journal of Petrology, 22, 553–583.

——— (1984) Magma mixing and magma plumbing systems in island arcs. Bulletin Volcanologique, 47, 685–703.

Smith, R.L. (1979) Ash-flow magmatism. Geological Society of America Special Paper 180, 5–27.

Spear, F.S., and Kimball, K.L. (1984) RECAMP—A FORTRAN IV program for estimating Fe^{3+} contents in amphiboles. Computers & Geosciences, 10, 317–325.

Spencer, K.J., and Lindsley, D.H. (1981) A solution model for coexisting iron-titanium oxides. American Mineralogist, 66, 1189–1201.

Spera, F., Yuen, D.A., and Kirschvink, S.J. (1982) Thermal boundary layer convection in silicic magma chambers: Effects of temperature dependent rheology and implications for thermogravimetric chemical fractionation. Journal of Geophysical Research, 87, 8755–8767.

Stormer, J.C., Jr. (1975) A practical two-feldspar geothermometer. American Mineralogist, 60, 667–674.

——— (1983) The effects of recalculation of estimates of temperature and oxygen fugacity from analyses of multicomponent iron-titanium oxides. American Mineralogist, 68, 586–594.

Vernon, R.H. (1983) Restite, xenoliths and microgranitoid enclaves in granites. Journal and Proceedings of the Royal Society of New South Wales, 116, 77–103.

Watson, E.B. (1979) Calcium content of forsterite coexisting with silicate liquid in the system Na_2O-CaO-MgO-Al_2O_3-SiO_2. American Mineralogist, 64, 824–829.

Whitney, J.A. (1975) The effects of pressure, temperature, and X_{H_2O} on phase assemblage in four synthetic rock compositions. Journal of Geology, 83, 1–31.

Williams, H. (1942) The geology of Crater Lake National Park, Oregon, with a reconnaissance of the Cascade Range southward to Mount Shasta. Carnegie Institution of Washington Publication 540, 162 p.

Wones, D.R. (1972) Stability of biotite: A reply. American Mineralogist, 57, 316–317.

——— (1981) Mafic silicates as indicators of intensive variables in granitic magmas. Mining Geology, 31, 191–212.

Wright, J.E. (1982) Permo-Triassic accretionary subduction complex, southwestern Klamath Mountains, northern California. Journal of Geophysical Research, 87, 3805–3818.

Yoder, H.S., Jr., and Tilley, C.E. (1962) Origin of basalt magmas: An experimental study of natural and synthetic rock systems. Journal of Petrology, 3, 342–532.

MANUSCRIPT RECEIVED OCTOBER 9, 1986
MANUSCRIPT ACCEPTED MAY 26, 1987